Chapter 5

Diffusion

5-1. Diffusion: thermal motion in viscous media

Diffusion is movement of solute and water molecules by random thermal, Brownian motion; the motion results from the impact of one molecule hitting another, imparting momentum. The random motions of a spherical molecule in a uniform medium have the same statistical properties in all directions; diffusion is normally *isotropic*. When the medium is structured, by a set of aligned macromolecules with parallel interstices between them, for example, a given energy produces higher-velocity motion parallel to the fibers than in the perpendicular direction; the diffusion is *anisotropic*. Diffusion is due to thermal motion: the molecular motion is proportional

to the temperature in degrees Kelvin: a 10° rise in temperature from 300° K to 310° K would cause only a 3% rise in diffusivity if other things remained constant. Diffusion is opposed by the viscosity of the medium: the more important effect of raising temperature is reducing viscosity and lowering the resistance to particle motion. Raising the temperature of water from 20 C to 30 C lowers its viscosity by almost 20%. See Table 5-1. The viscosity of water, 1 cP or 0.01

Table 5-1: Viscosity of water and air at 1 atmos pressure: $\upsilon = \eta / \rho$ (from Bird et al., 1960)

	WATER[a]		AIR[b]	
Temperature	Viscosity: η, cP	Kinematic Viscosity $\upsilon \cdot 10^2$ $\mathbf{cm^2 s^{-1}}$	Viscosity: η, cP	Kinematic Viscosity $\upsilon \cdot 10^2$
0	1.787	1.787	0.01716	13.27
20	1.0019	1.0037	0.01813	15.05
40	0.6530	0.6581	0.01908	16.92
60	0.4665	0.4744	0.01999	18.86
80	0.3548	0.3651	0.02087	20.88
100	0.2821	0.2944	0.02173	22.98

a. Calculated from the results of R.C. Hardy and R. L. Cottington, J. Research Nat. Bur. Standards, **42**, 573-578 (1949), and J. F. Swindells, J. R. Coe, Jr. and T. B. Godfrey, J. Research Nat Bur. Standards, **48**, 1-31, (1952)

b. Calculated from "Tables of Thermal Properties of Gases," Nat. Bur. Standards Circ. **464** (1955), Chapter 2.

g cm^{-1} s^{-1}, is about 100 times that of air. The kinematic viscosity, $\upsilon = \eta/\rho \cdot$ $cm^2 s^{-1}$, viscosity per unit density, is about 10 times higher for air than for water, simply because the density of air is so low, about 1.205 g/liter at 20° C. Kinematic viscosity has the same units as a diffusion coefficient. Note that the viscosity of fluids decreases with increasing temperature, but that gasses do the reverse.

Net diffusional fluxes occur by the net movement of particles from a locale of high concentration to one of lower concentration by this random movement of particles. Diffusion dissipates gradients, so concentrations tend toward equilibrium. (Entropy is raised by the dissipation of concentration gradients.)

Diffusion is thermal motion, usually random, and hindered by collisions with other molecules. It is slower in high-viscosity fluid. Water density, ρ, is 1 g/ml, and its viscosity is 1 cP. Diffusion in gases is much more rapid than in fluids since the density of molecules is much less: molecular spread of an aromatic substance can be smelled across a room in seconds, even if given little convective assistance. The density of dry air at 273° K is 1.29 kg/m^3 or 1.29×10^{-3} g/cm^3, one one-thousandth of that of water. The viscosity of dry air is 1.72×10^{-4} g cm^{-1} s^{-1} or 0.0172 cPoise (*CRC Handbook of Tables for Applied Engineering Science, Second Edition,* 1973), about one-sixtieth of that of water.

A common laboratory demonstration of diffusion involves layering solvent water carefully over a solution of deep blue copper sulfate, which has a higher density than water so the layers do

not mix (Fig. 5-1). Initially the layering gives a sharp boundary, across which the solute concentration changes abruptly from zero above to a value C_o below the interface. Immediately, random Brownian motion of the molecules begins and gradually blurs the boundary so that the gradation in color spreads. Only after a very long time in a graduated cylinder sitting on the classroom shelf for months does this lead to complete mixing and a uniform blue color. Thermodynamics says that mixing will eventually occur: the initial state is certainly not one of equilibrium; free energy will be lower, and entropy higher, when mixing is complete. Neglecting small contributions from the heat of mixing, the free energy change results entirely from the higher entropy of the mixed state.

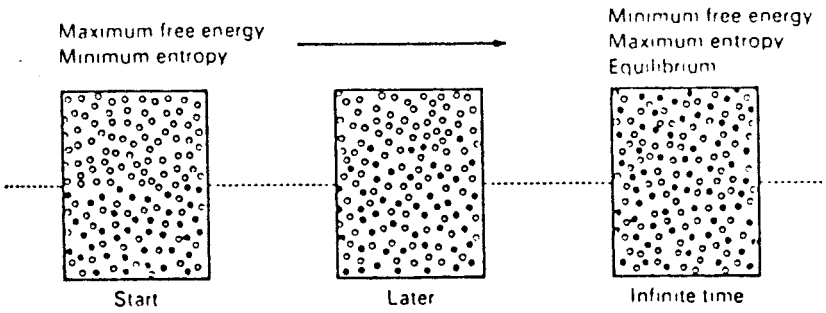

Figure 5-1: Diffusion of solute and solvent. Open circles are solvent; filled circles are solute. At the start, solute is in the bottom half of the fluid, but eventually the concentration becomes uniform throughout, and no concentration gradients remain. Solvent diffuses into the solution, net from above to below; net solute diffusion moves in the opposite direction.

5-1.1. Brownian movement and diffusion

Measurement of the change of position of a hard spherical particle in any *one* dimension will allow calculation of the diffusion coefficient and of the particle radius. The dominating condition is that the particle concentration be very low, which means that the effective viscosity is the viscosity of the pure solvent. The mean value of the square of the distance $(\Delta x)^2$ travelled along the x-axis in a chosen time interval, Δt, is obtained and the effective diffusion coefficient $D = (\Delta x)^2/2\Delta t$. Substituting into this the Stokes-Einstein relation, $D = RT/ 6\pi a\eta \aleph$, gives an experimental approach to estimating the effective molecular radius, *a,* when the viscosity of the medium, η, is measured separately:

$$(\Delta x)^2/\Delta t \;=\; 2D\,;\text{ or } (\Delta x)^2 \;=\; \frac{RT}{\aleph}\cdot\frac{\Delta t}{3\pi\eta a}\,. \qquad (5\text{-}1)$$

The frictional coefficient is $f_s = 6\pi a\eta$, for the molecule with the medium, assuming sphericity.

Saxby (1923**??**) used this method, as in Fig. 5-2, with *Staph. aureus* (diameter = 1.12 μ), to find $\aleph$, Avogadro's number, obtaining a value of 6.08×10^{23} (correct value = 6.023×10^{23}).

5-1.2. Diffusion coefficients

The diffusion coefficient, *D*, is not a physical constant but an observed phenomenological coefficient. Its dependence on particular features is indicated by the Einstein-Stokes expression,

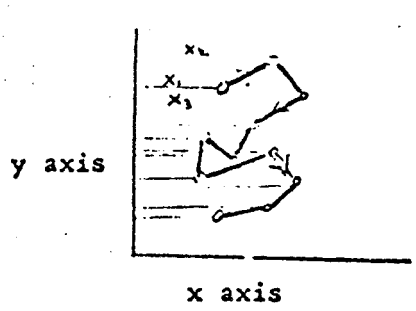

Figure 5-2: Calculation of D from Brownian motion. Saxby observed the x-positions of a spherical bacterium every 30 seconds, and calculated D and $\aleph$, Avogadro's number, using Eq. 5-1.

$$D = \frac{RT}{6\pi a \eta \aleph} \quad \text{or} \quad \frac{RT}{f \aleph}.$$

In this expression the energy per molecule is $RT/\aleph$, and the friction per molecule is $6\pi a\eta$, or f, and is equivalent to a force divided by a velocity, (g cm s^{-2})/ (cm s^{-1}).
Because the denominator contains the molecular radius a, the equation suggests that D might vary inversely with the reciprocal of (molecular weight)$^{1/3}$ but over a large range a square root relationship is closer for small molecules with MW < 4000 Daltons, but a cubic relationship is better for larger molecules. Some diffusion coefficients for important biological molecules are listed in Table 5-2.

Correction to $T = 20°$ C (293.2° K) was made by correcting for T and η from the value observed at $T°$ K:

$$D_{20} = \frac{293.2}{T} \frac{\eta_T}{\eta_{20}} D_T . \tag{5-2}$$

This does not correct for changes in molecular size such as occur with unfolding of the molecule or change in the degree of hydration. The viscosity η is the most important variable influencing D.

Proteins vary in their density and density's reciprocal measure, specific fractional volume, ml/g protein over only a small range, most being around 0.72 ml/g or a density of 1.39 g/ml.

Eq. 5-1 can be used to estimate the diffusion coefficients for substances when the data are not available, using inference from observed substances. For example the diffusion coefficient for CO_2 in air at 20° C is 2.45 $cm^2 s^{-1}$. To estimate the diffusion coefficient in air for methyl salicylate (Wintergreen, used in liniment), one could calculate the Stokes radii for both CO_2 and methylsalicylate. Alternatively, simply take the square root of the ratio of molecular weights, as an approximation to the ratio of Stokes radii, a(MeS)/a(CO_2), and substitute into the Stokes-Einstein relationship directly:

$$D_{MeS} = D_{CO_2} \cdot \sqrt{\frac{MW_{CO_2}}{MW_{MeS}}} = 2.45 \cdot \sqrt{\frac{44}{152}} = 1.32 cm^2 s^{-1}, \tag{5-3}$$

Table 5-2: Diffusion Coefficients in Water, D_w (in aqueous solution at 20°C)

Substance	Molecular Weight (g/mole)	$D_w \times 10^6$ (cm^2/sec)	Molecular Radius a or a,b (Å)	Specific Volume $\bar{v}$ (cm^3/g)
H_2	2	52		
H_2O	18	20		
O_2	32	19.8		
CO_2	44	17.7		
KCl	76.5			
NaCl	58.5	13.9		
Urea	60	11.8		
Glycine	75	9.335		
Glucose	180	6		
Sucrose	342	4.586		
Inulin	5,000	1.0		
Lysozyme	14,400	1.12		0.703
Bovine serum albumin	66,500	0.603		0.734
Hemoglobin	65,485	0.6		
Albumin	68,000	0.6	70 by 30	0.733
Tropomyosin	93,000	0.224		
Fibrinogen	330,000	0.202		0.723

assuming that the viscosity of the air is not changed by the presence of the odor. This method is pretty crude, but will still be quite good if the comparison can be made with a molecule of closely similar molecular weight. Attempting to calculate gaseous diffusion coefficients from aqueous ones using substitution for the viscosities of gas versus liquid doesn't work. The estimates for gaseous diffusion coefficients are 100-fold too low. Bird, Stewart and Lightfoot (1960, 2001) present an accurate theoretical approach, the Chapman-Enskog theory, which works well over a wide range of temperatures and pressures.

5-1.3. Influences of molecular shape on diffusion coefficients

The computation of frictional coefficients has been achieved by analysis of continuous systems, for example, Stoke's law:

$$f = 6\pi\eta a, \tag{5-4}$$

where f is the coefficient for friction between solute and solvent, a is the radius of a spherical particle and η is viscosity of the medium. For simple nonspherical shapes other estimates of f were obtained from hydrodynamic expressions. Examples of the effects of molecular asymmetry

Table 5-3: Frictional coefficients[a]

Shape	Frictional Coefficient	Explanation
Sphere	$f = 6\pi\eta R$	R = sphere radius
Prolate ellipsoid	$f = 6\pi\eta R_p \dfrac{(1-b^2/a^2)^{1/2}}{(b/a)^{2/3}\ln\{[1+(1-b^2/a^2)^{1/2}]/(b/a)\}}$	$2a$ = major axis, $2b$ = minor axis, R_p = radius of sphere of equal volume = $(ab^2)^{1/3}$
Oblate ellipsoid	$f = 6\pi\eta R_0 \dfrac{(b^2/a^2-1)^{1/2}}{(a/b)^{2/3}\tan^{-1}(a^2/b^2-1)^{1/2}}$	$2b$ = major axis, $2a$ = minor axis, R_0 = radius of sphere of equal volume = $(a^2b)^{1/3}$
Long rod	$f = 6\pi\eta R_r \dfrac{(b/a)^{1/2}}{(3/2)^{1/3}\{2\ln[2(a/b)]-0.11\}}$	a = half-length, b = radius, R_r = radius of sphere of equal volume = $(3b^2a/2)^{1/3}$

a. See Tanford 1961

are shown in Fig. 5-3. Although such analyses cannot take into account the asymmetric and often

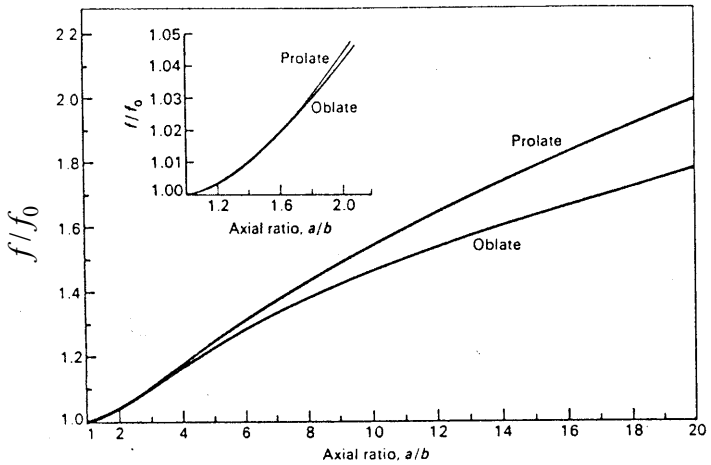

Figure 5-3: The dependence of frictional coefficient on particle shape. The ratio f/f_0 is the frictional coefficient of an ellipsoid of the given axial ratio divided by the frictional coefficient of a sphere of the same volume as the ellipsoid. (From Van Holde, 1971.)

very irregular shapes of molecules, and completely ignore the effects of random collisions or of molecular orientation in a field, the estimates are certainly useful. Deviations from sphericity increase *f* since the radius of rotation is necessarily increased by any deviation from spherical. Elongate molecules have much reduced diffusion coefficients in free solution. (Long change molecules, however, can penetrate fiber matrices and small pores by "reputation", a phrase chosen by De Gennes who envisaged the snake-like head-forward motion of a molecule through a hindered medium.) Of some relevance are the computations of Levitt (1975), who showed that diffusion modeling by the Markov processes representing the quantum mechanical expressions gave results essentially indistinguishable from those of hydrodynamic modeling for porous transport using continuum mechanics.

5-2. Fick's "Laws"

5-2.1. Fick's First Law of motion

Fick's First Law, for the flux due to diffusion across a plane in one dimension, is

$$\text{Net flux per unit area} = J_D = (1/A)\frac{dq}{dt} = -D\frac{dC}{dx}\ , \tag{5-5}$$

where J_D = diffusional flux per unit area, moles/(sec cm^2); q = amount, moles; t = time, sec; D = diffusion coefficient in the region, cm^2/sec; A = area available for diffusion, cm^2. The driving force is the spatial gradient in concentration or, more properly, in activity.

Consider a steady-state situation where there are two oceans of instantaneously stirred fluids with concentrations C_1 and C_2, separated by a stagnant region of thickness Δx, as in Fig. 5-4. Then in steady state the net flux = $\Delta q/\Delta t = -DA(C_2 - C_1)/\Delta x$. Here a conductance, L, equals DA and the driving force $\Psi = \Delta C/\Delta x$. Fick's First Law says ΔC tends toward zero.

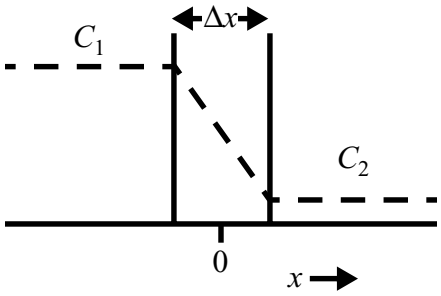

Figure 5-4: Fick's First Law of diffusion through a stagnant region in steady state.

As an aside, when the membrane is thin, Δx goes to 0, and the system can be represented by ordinary differential equations in which the two chambers have volume V_1 and V_2:

$$\frac{dC_1}{dt} = \frac{D_m A_m}{\Delta x \cdot V_1} \cdot (C_2 - C_1) = \frac{P_m A_m}{V_1} \cdot (C_2 - C_1), \tag{5-6a}$$

defining the membrane permeability $P_m = D_m/\Delta x$, cm/s. Likewise the equation for the second chamber is:

$$\frac{dC_2}{dt} = -\frac{P_m A_m}{V_2} \cdot (C_2 - C_1) \tag{5-6b}$$

To derive the flux equation, Eq. 5-5, from the general statement, a flux equals a conductance times a driving force, $J = L\Psi$, one goes back to the principle that the gradient in activity (chemical potential), $\partial\mu_s/\partial x$, is the driving force for solute:

$$J_s = -L_s \partial\mu_s/\partial x\,, \tag{5-7}$$

where L_s is the conductance for the solute. The chemical potential of the solute depends on temperature, pressure, and the concentration. T and P are assumed to be uniform, so there is no change in the activity coefficient with position along the gradient, under which

$$\frac{\partial\mu}{\partial x} = \left(\frac{\partial\mu}{\partial C}\right)_{T,P} \frac{\partial C}{\partial x}\,. \tag{5-8}$$

conditions the *concentration gradient* determines the flow. When the activity coefficient, ϕ_s, is concentration-dependent as described in the previous chapter, then $\partial\mu/\partial C$ must be expanded to account for changes along the gradient:

$$(\partial\mu/\partial C)_{T,P} = (RT/C)[1 + C(\partial \ln\phi_s/\partial C)]\,; \tag{5-9}$$

$$J_s = -\frac{L_s RT}{C}\left(1 + C\frac{\partial \ln\phi_s}{\partial C}\right)\frac{\partial C}{\partial x}\,. \tag{5-10}$$

The conductance per unit concentration, L_s/C in Eq. 5-10 can be replaced by $1/\aleph f_s$, the reciprocal of the molecular frictional coefficient times the number of molecules:

$$J_s = -\frac{RT}{\aleph f_s}\left(1 + C\frac{\partial \ln\phi_s}{\partial C}\right)\frac{\partial C}{\partial x}\,, \tag{5-11a}$$

$$\text{or when the activity is constant,} \quad J_s = -D\frac{\partial C}{\partial x}. \tag{5-11b}$$

This defines D, the *diffusion coefficient*, as

$$D = \frac{RT}{\aleph f_s}\left(1 + C\frac{\partial \ln\phi_s}{\partial C}\right) = \frac{RT}{\aleph f_s} \text{ in dilute solution.} \tag{5-12}$$

From an experimental point of view, D is defined by Eq. 5-11b, called *Fick's First Law*. Eq. 5-11b is in accord with our intuitive expectation that the flux will cease only when the concentration gradient has vanished. Eq. 5-12 demonstrates that D depends on three factors: RT, which may be taken as a measure of the kinetic energy of the molecules, a correction term, $[1 + C(\partial \ln\phi_s/\partial C)]$,

expressing the fact that the chemical potential depends on solute-solute interaction, and thirdly, on the size and shape of the molecule, reflected in the frictional coefficient, f_s.

For ideal solutions we may neglect the activity coefficient factor and obtain $D = RT/\aleph f_s$ which reduces to $RT/\aleph 6\pi a\eta$ for spheres. If, in addition, η does not vary significantly with local differences in solute concentration, D is a constant.

5-2.2. Fick's Second Law of diffusion

At a given point, x, this law expresses the rate of change of concentration with respect to time as a function of the concentration gradients adjacent to this point, as in Fig. 5-5. By differentiating Eq. 5-11b (Fick's First Law) with respect to distance, and substituting from the equations of continuity, we obtain

$$\frac{\partial C(x,t)}{\partial t} = D\frac{\partial^2 C}{\partial x^2} \quad . \tag{5-13a}$$

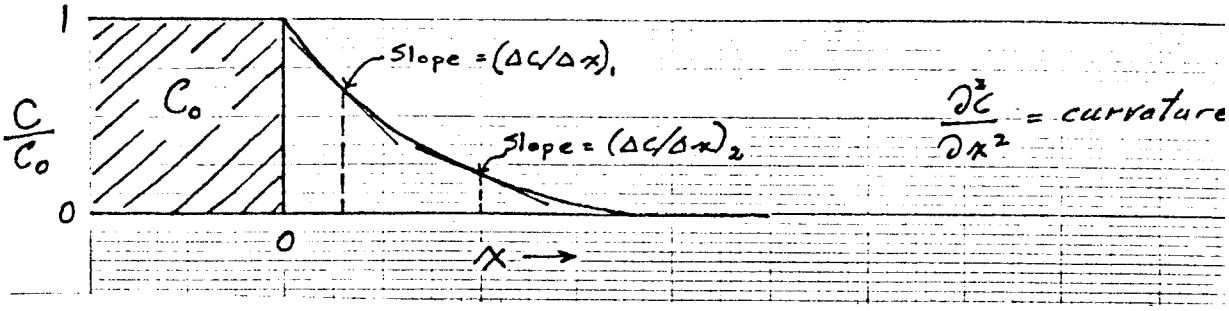

Figure 5-5: Fick's Second Law. The graph depicts the diffusion from an ocean of fixed concentration at $x < 0$ into a medium where $C(x) = 0$ initially and the front advances with time.

Over a small finite distance $x_2 - x_1$ the rate of concentration change is approximated by

$$\Delta C/\Delta t = D[(\Delta C/\Delta x)_2 - (\Delta C/\Delta x)_1]/(x_2 - x_1)\,. \tag{5-13b}$$

Fick's Second Law indicates that nonuniform gradients tend to become uniform (when D in the medium is uniform). This occurs at early times within a membrane with fixed concentrations on either side, eventually resulting in the straight profile seen in Fig. 5-6, considered next.

5-3. Measuring diffusion coefficients

5-3.1. Diffusion across a thick membrane

The Barrer time lag method for estimating *D*. In the experiment described by Barrer (1953) there is a thick membrane separating two well-mixed fluid regions. Solute is added to the left region at $t = 0$. Since the membrane contains no solute initially there must be a time lag before solute reaches the right region, and more time until there is the straight steady-state profile seen in Fig. 5-4. This is diagrammed in the left panel of Fig. 5-6, taken from the study of Safford et al.

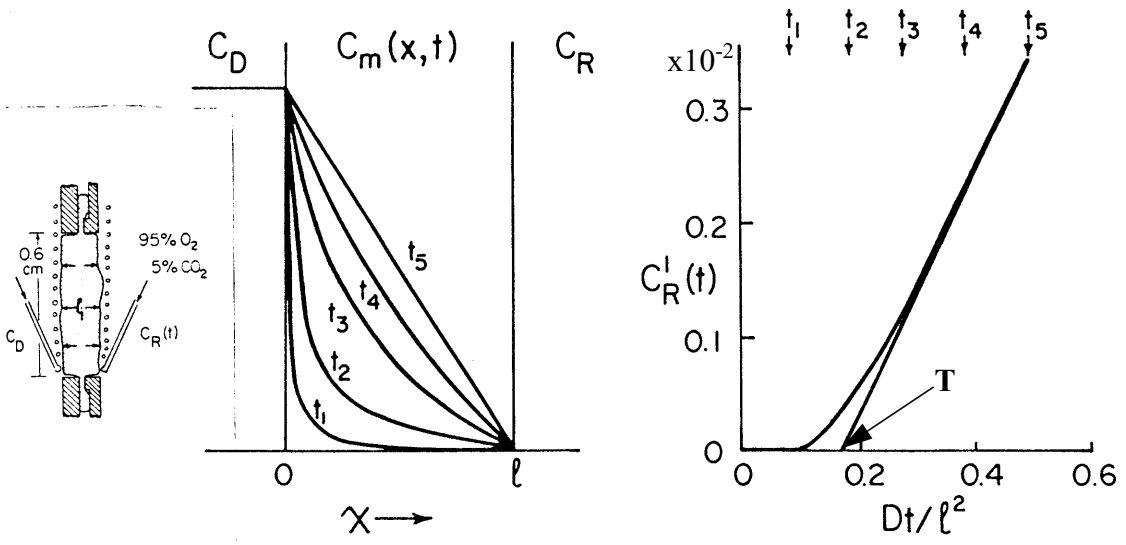

Figure 5-6: Transient in diffusion across a uniform slab of finite thickness. The experimental setup at left is used for example by Safford and Bassingthwaighte (1978) where stream of bubbles rising across the face of the sheet of tissue circulate fluid. Inside the tissue the gradients become uniform when changes in concentration on both the donor side C_D and the recipient side C_R are small prior to the time to reach a psuedo-steady state of linearly rising concentration. In the right panel is shown $C'_R = C_R/C_D$ for the condition $C'_R = 0$ at $t = 0$. The pseudo-steady state is approached at Dt/l^2 of about 0.5, diagrammed as t_5, where the profile is a staight line between $C_m = C_D$ at $x = 0$ and $C_m = C_R$ at $x = L$ and the actual recipient concentration is still less than 0.4% of that of the source in this particular case. (The linear region is the first part of an almost monoexponential rise to the equilibrium $C'_R = C_D$.

(1978) on the diffusional transport of tracer-labeled water through a sheet of heart tissue. The profiles $C(x)$ within the sheet of thickness l are curved until steady state has been reached at time t_5. The curvature takes time to dissipate, in accord with Fick's Second Law (Eq. 5-13a). Observations of the time course of solute concentration in the right region show a delay before any solute appears, then a gradually steepening rate of rise until the pseudo steady state is reached at about t_5. The time lag T introduced by Barrer is the intercept of the straight line fitted to the steady-state data and extrapolated back to the baseline. For a tissue of uniform properties and thickness, l, $D = l^2/6T$. The concentration in the right region, $C'_R = C_R/C_D$, is a small fraction of that in the source region on the left side and at time T is still only 0.1% of C_D so that the backflux from right to left is still negligible. The slope, dC_R/dt, also gives a measure of D when the membrane surface area and thickness are known: $V_R dC_R/dt = PA_m \Delta C = A_m(D/l)\,\Delta C$, where A_m is the membrane surface area, P is a permeability equal to D/l, and $\Delta C = C_D$ is the driving force, the concentration on the source side. The approach assumes that the volume, V_R, on right side will be large enough that C_R remains so much less than C_D that back diffusion from the right to the left side is negligible. Note the dimensionless time scale used for generality in the right panel of Fig. 5-6.

This method has been extended by Safford and Bassingthwaighte (1977) and Safford et al. (1978) to account for additional complexities commonly found in tissues: (1) heterogeneity of path length across the sheet of tissue, (2) the presence of immobile binding sites for solutes such

as calcium, and (3) for diffusion through and around cells distributed in interstitial fluid, with solute penetrating the cell membranes.

The Barrer equation for diffusion across a planar slab of tissue of thickness l (also given by Crank, 1975) is provided by a convergent series:

$$C'_{\mathrm{R}} = \frac{DAt}{Vl} - \frac{lA}{6V} - \frac{2lC_{\mathrm{D}}A_{\mathrm{d}}}{\pi^2}\sum_{\mathrm{m}=1}^{\mathrm{m}=\mathrm{M}}\frac{(-1)^{\mathrm{m}}}{m^2}\exp\left(\frac{-Dm^2\pi^2 t}{\lambda^2 l^2}\right), \tag{5-14}$$

where D is the apparent diffusion coefficient, cm^2/s; A is area, cm^2; t is time, seconds; V is volume of the right or recipient chamber, ml; l is slab thickness, cm. At $t = T$, the time intercept,

$$D = \frac{l^2}{6T}. \tag{5-15}$$

When a pseudo steady state is reached, that is, when the transient terms have vanished and the slope dC'_R/dt, becomes constant, another measure of D is obtained:

$$D = \frac{Vl}{A}\cdot\frac{d}{dt}C'_{\mathrm{R}}. \tag{5-16}$$

5-3.2. Diffusion across an interface between unstirred regions

This is the basis of a technique commonly used for measuring diffusion coefficients in gels, cells, or tissues. The usual approach is to label one region uniformly with tracer and to allow time for the tracer to diffuse into the neighboring region; in Fig. 5-7 the region where $x < 0$ is initially free of tracer.

The random nature of the diffusion process is re-emphasized by the fact that the solution for Eq. 5-13a gives the Gaussian error curve for dC/dx, the curve to the right in Fig. 5-7:

$$\frac{\partial C}{\partial x} = \frac{C_{\mathrm{o}}}{2(\pi Dt)^{1/2}}\cdot e^{-x^2/4Dt}. \tag{5-17}$$

The standard deviation, SD, of $\partial C/\partial x$ is $2\sqrt{Dt}$ and its height, ∂C at $x = 0$, is $C_o/2(\pi Dt)^{1/2}$ or $0.3998\ C_o/\mathrm{SD}$. The SD increases with the square root of time. The area under $\partial C/\partial x$ from $-\infty$ to $+\infty$ is C_o, so that as the solute disperses the curve shape remains Gaussian and the area constant, but the ratio $(\text{area/height})^2$ increases linearly as in Fig. 5-8.

$$\frac{\text{area}}{\text{height}} = 2(\pi Dt)^{1/2} = 2.507\times SD. \tag{5-18}$$

This provides a direct estimate of D = (slope, $(\text{area/height})^2/\mathrm{dt})/4\pi$.

An approach similar to that in Fig. 5-7 is to label a thin cross-section at $x = 0$. In the ideal situation, an infinitely thin section, $C(x)$, will have the form that $\partial C/\partial x$ has in Fig. 5-7; that is, impulse labeling (with respect to distance x) has a response which is the derivative of step

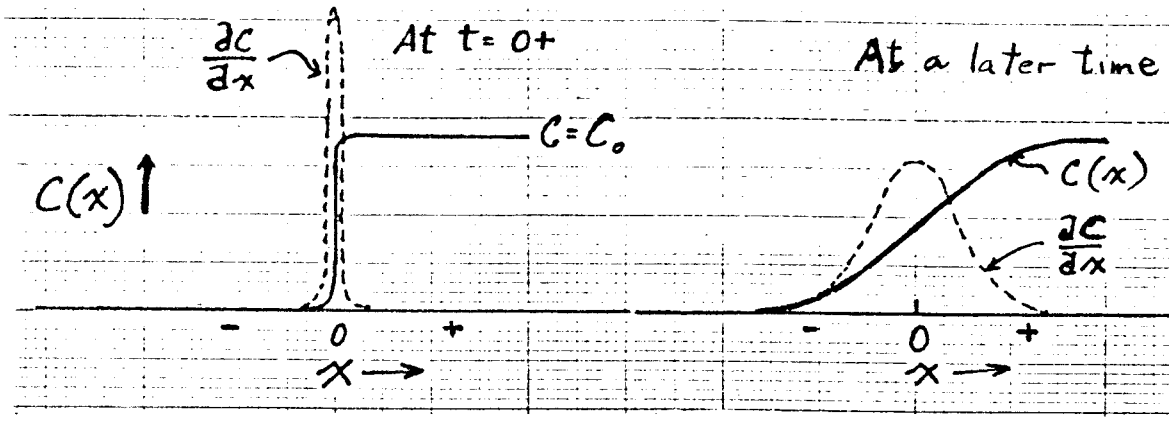

Figure 5-7: Diffusion across an interface into a stagnant region. The diffusion coefficients are assumed the same in the source region as in the stagnant region.

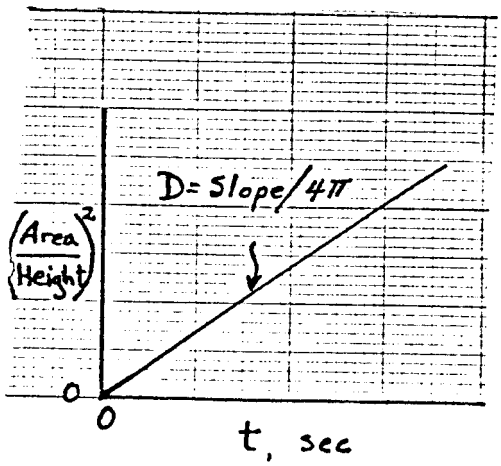

Figure 5-8: Determination of diffusion coefficient from plot of (area/height)^2 of $\partial C/\partial x$ from an experiment such as that in Eq. 5-7. There is a slightly positive ordinate intercept due to a small amount of dispersion present at $t = 0$ due to imperfections at the interface.

function labeling. (This is completely analogous to the relationship between system responses following impulse inputs and step inputs.)

5-4. Applications to biological situations

5-4.1. Flux by diffusion across a uniform membrane depends on solubility

Solubility in a lipid membrane is increased by alkyl groups and decreased by polar groups (–OH, –COOH, NH_2). The partition coefficient, λ, is the ratio of its lipid solubility to water solubility:

$$\lambda = C_{\text{membrane}} / C_{\text{medium}} . \tag{5-19}$$

In the situation diagrammed in Fig. 5-9 the gradient across the membrane is not provided by the concentrations at the surfaces, but by those within the membrane, $\Delta C_m = \lambda C_2 - \lambda C_1$:

$$J_s = -D_m \frac{\Delta C_m}{l}, \tag{5-20a}$$

where J_s is the net flux of solute from side 1 to side 2. To be more explicit, it might be written as

$$J_s = J_{S_{net12}} = J_{12} - J_{21} = -D_m \frac{\lambda(C_2 - C_1)}{l}. \tag{5-20b}$$

In Eq. 5-20b the driving force is rewritten in terms of the observed solution concentrations times the membrane-to-solution partition coefficient. In many situations where D_m, λ, and l are unknown (as with most biological membranes), then an observed flux with a known concentration difference provides an estimate of the combination of factors lumped together as a permeability:

$$J_s = -P\Delta C \quad \text{where} \quad P = D_m \lambda / l. \tag{5-21}$$

Examples of membrane/water partition coefficients for biological membranes are glycerol, 10^{-4}; urea, 10^{-4}; ethanol, 10^{-2}; triethylcitrate, 1; dimethylsulfoxide, 200.

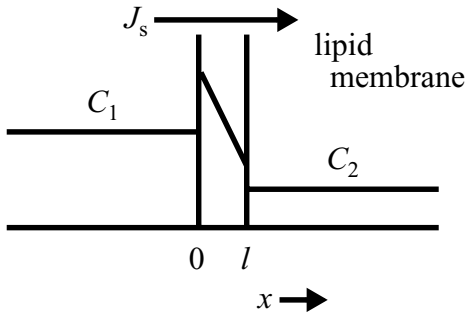

Figure 5-9: Diffusion across a nonporous membrane. C_1 and C_2 are concentrations in well-stirred aqueous oceans. $\lambda = 1.5$. The gradient dC_m/dx is greater than $(C_1\text{-}C_2)/l$ when $\lambda > 1$, thus high membrane solubility augments permeation.

5-4.2. Diffusion through pores

1. *Large pores* in an otherwise impermeable membrane can be treated as if there were free diffusion through a fraction of the membrane. This generally applies to smaller solutes and membranes with large water contents. The flux of solute is given by

$$J_s = -D_w \left(\frac{A_p}{A_m}\right) \frac{\Delta c}{l}, \tag{5-22}$$

where D_w is the diffusion coefficient in water, A_p/A_m is the pore area as a fraction of the membrane area, and l is the membrane thickness. (Again J_s is moles s^{-1} cm^{-2} and Δc is the difference in concentrations on the two sides of the membrane.)

2. *Small pores* have additional effects due to (i) entrance effects, (ii) friction between pore wall and solute, and (iii) solute-solute and solute-solvent interactions. The entrance effect in its simplest form can be regarded as exclusion of the center of the molecule from any position closer to the wall than the molecular radius, as in Fig. 5-10:

$$\text{effective pore area} = A_p(1 - a/r_p)^2 .$$

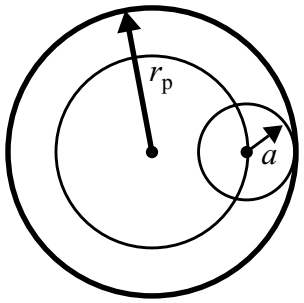

Figure 5-10: Cross-sectional area of pore available to solute is less than the pore area. The effective pore area is A_p $(1- a/r_p)^2$.

This reduction in available volume for solute within a pore has the effect of reducing its average concentration relative to that in free solution outside the pore. This is equivalent to other mechanisms of molecular exclusion, and is the same thing causing reduction in hematocrit in capillaries relative to that in large vessels, that is, due to the fact that red blood cells cannot be centered at the wall.

If a cell is dumped into medium containing D_2O then the concentration inside rises rapidly. The transport rate of D_2O is about 1% of that through a similar thickness of water and suggests that only 1% of the surface is available for D_2O transport. Therefore, consider aqueous pores totalling 1% of the area of surface, or solubility of D_2O in membrane being 1% of solubility in H_2O. These are probably mainly aquaporin channels (Agre et al., 1993).

Good reviews on porous transport are those of Bean (1972), Curry (1984), and Deen (1987). For reviews of solute transport through hindered matrices see the excellent chapter in the *Handbook of Physiology* by Curry (1984), the two volume book by Comper (1996a, b) on the extracellular matrix, and articles by Nugent and Jain (1984) and Tong and Anderson (1996). Porous transport will be covered in greater detail in Chapter 6.

5-4.3. Diffusion across walls and pores in parallel

Now consider the membrane to have a fraction of the area that has the area of a set of pore, A_p/A_m, and the other fraction being a normal lipid bilayer with fractional area 1 - A_p/A_m, The latter fraction is N_{pore}. $\pi r^2/A_m$. Then J_s is the sum of the two fluxes in parallel, per unit membrane area.

$$J_s = J_{pores} + J_{membrane} \tag{5-23a}$$

$$= -D_{pore}\left(\frac{A_p}{A_m}\right)\frac{\Delta C}{l} - D_m\left(1 - \frac{A_p}{A_m}\right)\lambda\frac{\Delta C}{l}$$

$$= -\left[\frac{D_{pore}}{l}\left(\frac{A_p}{A_m}\right) + \lambda\frac{D_m}{l}\left(1 - \frac{A_p}{A_m}\right)\right]\Delta C$$

$$= -(P_{pore} + P_{membrane})\Delta C \quad , \tag{5-23b}$$

where P_{pore} and $P_{membrane}$ are defined by the expressions on the line preceding.

Since A_p/A_m is usually very small for cell membranes, the product of the partition coefficient λ times D_m is the major determinant of the flux. The D_{pore}/l is determined by the nature of the pores and the solutes, as discussed in Chapter 6-7, and is here written as if there is no steric hindrance.

5-4.4. Diffusion from a stirred infinitely large source into a non-consuming stagnant region

First consider diffusion into a plane sheet of unstirred isotropic material of thickness $2l$ and containing no obstructions or binding sites. The initial concentration in the plane sheet is C_0; at $t = 0$ the concentrations at the two surfaces are set to C_1. Fig. 5-11 depicts the concentration profiles within the slab at a succession of normalized times, Dt/l^2, as solute diffuses in and eventually equilibrates with the external concentration on each side. At early times these curves are the same shape as those for low values of Dt/l^2 in Fig. 5-6.

Patlak and Fenstermacher (1975) used a similar method for measuring diffusion into brain tissue which was dependent on maintaining a constant concentration within the cerebral ventricles, which they perfused, and, after sectioning the brain and measuring concentration as a function of distance from the surface, observed the profiles shown in Fig. 5-12. Since the profiles were all close to the surface this is effectively one-dimensional diffusion from a constant source into an infinite region. The profiles do not become constant since solute continues to enter. "Infinitely large source" implies that there is no apparent depletion of the solute concentration within the source. Observation of the concentration profile within the brain was interpreted in terms of the expression for one-dimensional diffusion, giving $C(x)$ where x is the distance from the surface:

$$\frac{C(x)}{C_o} = \text{erfc}\frac{x}{2(Dt)^{1/2}}. \tag{5-24}$$

(Note that the ordinate scale in Fig. 5-12 is erfc, not exponential.) The complementary error function, erfc, is 1.0 minus the integral of the Gaussian pdf (probability density function). that is, is 1.0 minus the integral of $(1/((2\pi)^{0.5}\sigma) \cdot \exp(-x^2/2\sigma^2)$, and $\sigma = (Dt)^2$. The profiles in Fig. 5-12 have the shape of the integral of $C(x)$ in Fig. 5-7. (Extend the analogy to time responses: this is analogous to a ramp input function, the integral of the step input function.) The profile continues to change with time, an unreal situation, since Eq. 5-24 assumes the stagnant region is also infinite, and x may increase without limit.

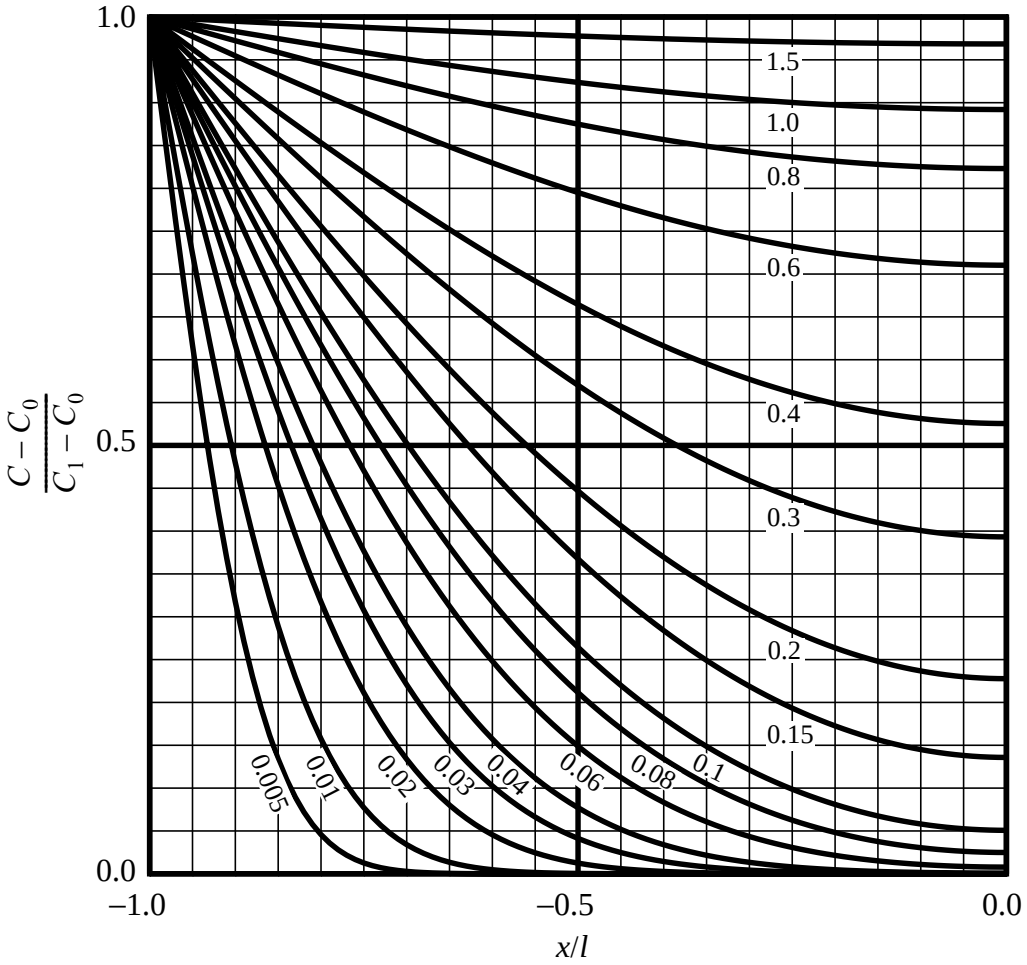

Figure 5-11: Diffusion into a plane sheet of thickness 2 l at various times after exposure to C_o at both surfaces. Concentration distributions at various times in the sheet $-l < x < l$ with initial uniform concentration C_o and surface concentration C_1. Numbers on curves are values of Dt/l^2. No consumption of solute. (After Crank, 1956.)

5-4.5. Diffusion into a region with solute consumption

The concentration profiles do become constant if there is consumption within the tissue, or if the tissue thickness x is finite. If the consumption is first-order (that is, in proportion to the concentration), then Eq. 5-13a has an additional term:

$$\frac{\partial C}{\partial t} = D\frac{\partial^2 C}{\partial x^2} - KC, \tag{5-25}$$

where K is a fractional clearance, ml · (ml tissue)$^{-1}$ s^{-1}. The clearance K can be due to loss by permeation from the tissue into capillaries or by a first order metabolic consumption. At high K the concentrations exponentially approach zero.

When the consumption is zero-order, that is, uniform throughout the tissue, calculations can only be made for regions where sufficient solute is available. For a thin sheet of muscle with uniform O_2 consumption, at steady state the conditions are

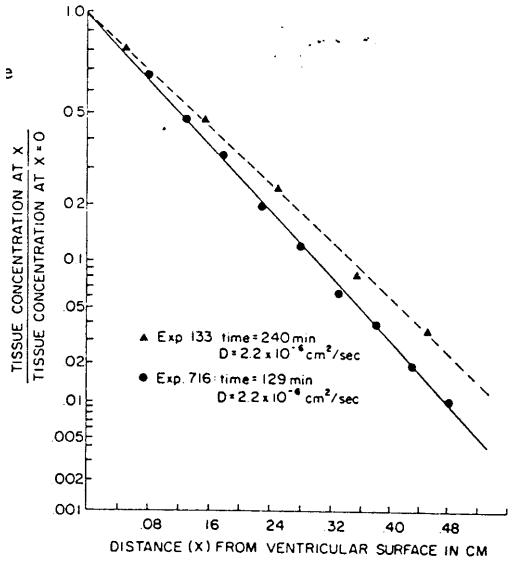

Figure 5-12: One-dimensional diffusion from a constant source into an infinite region. The profiles do not become constant since solute continues to enter. Inverse complimentary error function graph of ^{14}C-creatinine tissue concentration profiles in dog caudate nucleus after two different methods of perfusion. (From Patlak and Fenstermacher, 1975.) The complementary error function, erfc, Eq. 5-24, is 1.0 minus the integral of the Gaussian pdf given in Eq. 5-17. (Note that the graph ordinate scale is erfc, not exponential.)

$$\frac{\partial^2 C}{\partial x^2} = \frac{K'}{D}, \tag{5-26}$$

where K' is the zero-order consumption in moles · (ml tissue)$^{-1}$ · s^{-1} independent of the concentration, $C(x)$. The resultant profiles, Fig. 5-13, are parabolas. The maximum depth that can be supplied is dependent on the concentration at the surface relative to the consumption. In this situation the concentrations become truly zero in the regions where utilization exceeds influx.

Patlak and Fenstermacher (1975) observed that the profiles became stable when the cerebral ventricles were perfused with ^{14}C-urea solution, shown in Fig. 5-14, in contrast to the situation for creatinine shown in Fig. 5-12. The difference is due to the loss of urea from the tissue into the blood perfusing the brain, through the capillary membranes, while creatinine does not cross the blood-brain barrier and therefore continues to diffuse deeper into the tissue.

5-5. Diffusion in Heterogeneous Media

5-5.1. Diffusion through ISF and cells in parallel and in series

Diffusion of gases and moderately hydrophilic solutes can occur both through and around cells in the ISF (interstitial fluid space). Heterogeneous diffusion occurs in gel matrices, especially for molecules large enough to be excluded from some of the water, in cellular tissues, in packed cell columns and in heterogeneous, multicellular tissues. In 1873, Maxwell worked out an equation

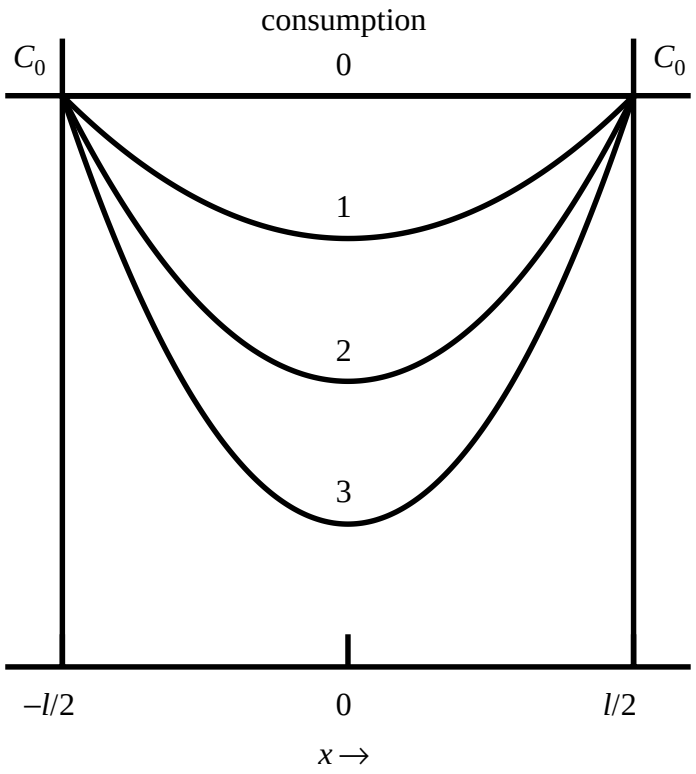

Figure 5-13: Steady-state profiles of concentration with zero-order consumption in a uniform sheet of thickness l are parabolic. Parameters for Eq. 5-26 were K', the zero-order consumption in moles · (ml tissue)$^{-1}$ · s^{-1} = 1, 2, and 3, the thickness l was x cm, D was y cm^2/s, and the surface concentration was z mM. (PARAMS)

for the effective bulk diffusion coefficient in the tissue, D_b, for the situation where diffusion occurs through both:

$$\frac{D_b}{D_e} = \frac{2D_e + D_i - 2\phi(D_e - D_i)}{2D_e + D_i + \phi(D_e - D_i)} \quad , \tag{5-27}$$

where D_e and D_i are extracellular and intracellular diffusion coefficients and ϕ is the cell volume fraction of the tissue. When $\phi = 0$, no cells, the right hand side is unity, so $D_b = D_e$. When $\phi = 1$, no interstitial space, $D_b = D_i$.

A modern example is diffusion across a slab of unperfused tissue, as seen in an experiment by Safford et al. (1978) in which they looked at the transport of tracer ^{3}HHO water (permeating and diffusing across cells as well as ISF) and sucrose (unable to permeate cell membranes and therefore restricted to the ISF). The formulation of the problem is similar to Maxwell's but incorporates a finite permeability of the cell membrane retarding the exchange between cells and interstitium. (In Fig. 5-15 the cells are diagrammed as square beams of infinite length.)

The calculation is for one-dimensional diffusion via two paths continuously connected: one path is via extracellular ISF only, and the other is through cells and ISF alternately. The cell-to-cell spacing L_o cm is the same laterally as axially, and is determined by the cell size L cm and the cytocrit, Cct, (the cell volume fraction, analogous to the hematocrit for RBC fraction of

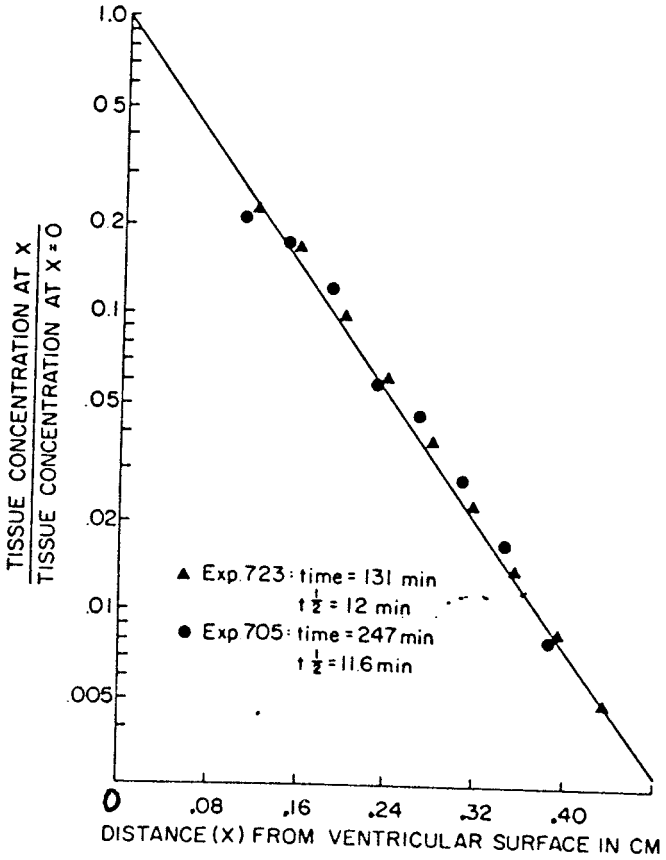

Figure 5-14: Diffusion profiles at steady state when solute is being uniformly consumed or removed from the tissue at various rates (Eq. 5-25). Semilogarithmic plots of 14C-urea tissue concentration profiles in dog caudate nucleus at two durations of ventriculo-cisternal perfusion with urea solution. (Patlak and Fenstermacher, 1975.)

blood) such that $L_o = L(1/\sqrt{Cct} - 1)$, as diagrammed in Fig. 5-15 (from Safford et al., 1978).For cardiomyocytes L is about 10 microns and with a cell volume fraction of 59%, L_o = 3 microns.

The experiment is diagrammed in Fig. 5-6 and the data on the tracer concentrations, $C_R(t)$, of ^{3}HHO and ^{14}C-sucrose are fitted using Barrer's Equation 5-14 to give an overall bulk diffusion coefficient, D_b, of 2.2×10^{-6} cm^2/s for each solute. From this result one estimates intracellular, D_i, and extracellular, D_e, diffusion coefficients and the cell membrane permeability, P cm s^{-1}, from anatomic data by translating the cell volume fraction ϕ into values of L and L_o, leaving only the D's as free parameters. Having data from a pair of tracers, one of which does not enter cells, the sucrose, further constrains the parameter estimates by defining diffusivity in the extracellular path. D_b is given by:

$$D_b = D_e\left\{\left(\frac{L_o}{L+L_o}\right) + \left[L\left(\frac{D_i}{D_e}\right)(W\alpha K - Q) - L_o(\alpha K + Q)\right]^{-1}\right\}^{-1}, \qquad (5\text{-}28)$$

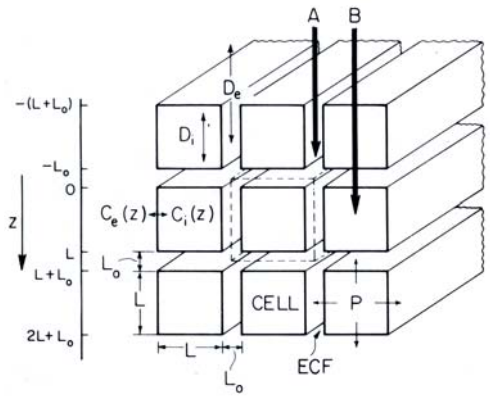

Figure 5-15: Diffusion in parallel through and around cells embedded in interstitial matrix. While Eq. 5-28 is specific for the square array of cells in this figure, the numerical solutions for the equations using hexagonal arrays of circular cells are virtually indistinguishable. (From Safford et al., 1978, their figure 4.)

$$\text{where } \alpha = \left[2P\left(\frac{1}{L \cdot D_\text{i}} + \frac{1}{L_\text{o} \cdot D_\text{e}}\right)\right]^{1/2}$$

$$E = L + D_\text{i}/P$$

$$F = [1 - \cosh(\alpha L)]/L + P(1 + W)/D_\text{i}$$

$$G = \sinh(\alpha L)/L + W\alpha$$

$$H = (1 + Y)/E + P(1 + W)/D_\text{i}$$

$$I = X/E - W\alpha$$

$$J = \frac{GH}{F} + I$$

$$K = \frac{1}{J}\left[\frac{1}{E} - \frac{H}{FL}\right]$$

$$n = D_\text{i}\alpha/P$$

$$Q = \alpha\left[KW - \frac{U(1 + W)}{n}\right]$$

$$U = \frac{1}{F}\left[\frac{1}{L} + GK\right]$$

$$W = \left(\frac{L_o}{L}\right)\left(\frac{D_e}{D_i}\right)$$

$$X = W[\sinh(\alpha L) + n\cosh(\alpha L)]$$

$$Y = W[\cosh(\alpha L) + n\sinh(\alpha L)]$$

Using these expressions for the analysis, they found that the bulk diffusion coefficient for water in heart muscle was 2.5×10^{-6}cm^2 s^{-1} or about 10% of the free diffusion coefficient in water, 2.38×10^{-5} cm^2 s^{-1} at the 23° C temperature of the experiments. The data suggested a cell surface permeability of 2 cm/s and intraregional diffusion coefficients of about 25% of the free aqueous diffusion coefficient both inside the cells and in the interstitial space. At the same time the sucrose (MW = 342 Daltons) diffusion coefficient in the interstitial space was 1.5×10^{-6}cm^2 s^{-1}, or 22.6% of the aqueous diffusion coefficient. Thus the tortuosity and steric hindrance of the interstitial matrix reduces the effective diffusion coefficient for small solutes in the ISF to one quarter of the free diffusion coefficient, and the intracellular diffusion of water is about as rapid as is extracellular, but low membrane permeability is a factor in reducing the rate of movement of tracer water to 10% of that in water.

In whole organ studies we observe (Yipintsoi and Bassingthwaighte 1970 #67; Bassingthwaighte and Beard 1995 #432) that water exchange is so fast in the heart that it is essentially flow-limited in its capillary-tissue exchange, which means that slowing of radial diffusion into the nearby cells cannot be detected. This is exactly what one would predict from the estimated P of 2 cm/s, since though measurable in the diffusion experiment is far higher than needed to explain very rapid exchange in an organ with high capillary density and short radial diffusion distances.

The extreme cases for Eq. 5-28 occur with the cell permeability P of either zero or infinity:

$$D_b(P = 0) = D_e \cdot \frac{L_o(L + L_o)}{L(L + L_o) + L_o^2}\ , \text{ and} \tag{5-29}$$

$$D_b(P = \infty) = \frac{1}{\dfrac{L}{LD_i + L_oD_e} + \dfrac{L_o}{(L + L_o)D_e}}\ . \tag{5-30}$$

Note that in Eq. 5-29 the $L(L + L_o)$ is the area for diffusion and is divided by the total area of the plane across which diffusion occurs. With other values being the same, $D_b\,(P = 0)$ would be 1.1×10^{-6} cm^2/s, and $D_b\,(P = \infty)$ would be 5.6×10^{-6} cm^2/s.

This computation improves upon a formula given by Redwood et al. (1974) because it accounts for exchange across the whole surface of the cells instead of only the part of the surface perpendicular to the diffusion front. When P = 0, Eq. 5-29 can be further reduced to illustrate that the result differs from Maxwell's formula by accounting for the absence of useful vertical diffusion in the horizontal spaces between the cells: this is simply a stagnant region, equivalent to a dead-end pore, when P = 0 so that:

$$D_b(\mathrm{P}=0) \;=\; D_e \cdot \frac{\phi - LL_0/(L+L_0)^2}{1 - LL_0/(L+L_0)^2}, \tag{5-31}$$

rather than simply $D_e\,\phi$. The same reduction with P = 0 would occur with the Redwood model.

This cell-interstitium model analysis is also applicable to the diffusion and exchange of oxygen in blood, where there is diffusion inside and outside RBC. Inside the RBC most of the oxygen is bound and diffuses as $Hb(O_2)_4$, where the high concentration gives a high intracellular transfer rate.

5-5.2. Diffusion across an uneven slab of tissue:

Copy in here the theory section of Suenson and ...JB #109 pages 1118 onward as edited by hand.

use figs 1,5,6 of suenson 1974

5-5.3. Diffusion through tissues with dead-end pores:

This is a situation analogous to one with fixed binding sites. Given a Barrer-type experiment, as in Fig. 5-6, instead of examining intratissue concentration profiles one has only the rising time course of concentrations in the unlabeled chamber, $C_R(t)$, to use to estimate the parameters of the diffusional system. Tissue sheets are usually non-uniform; the equations need therefore account for: heterogeneity of path lengths, diffusion into sequestered regions, volumes or binding affinities in those regions, and both intracellular and extracellular space. Following the derivation from Goodknight and Fatt (1961 #2251) for oil shales.....??

Here use the figure in Suenson 1974 jbb#109 fig 4

5-5.4. Diffusion through a hindering matrix

Rview sections of Curry and Michel and BSL re pointers for this.

5-6. Diffusion of solutes which can be bound to absorbing sites

Many small solutes bind to proteins; this is physiologically advantageous in a wondrous variety of circumstances. Fatty acids binds tightly to plasma albumin, occupying as many as seven binding sites and usually about three, and is about 99.94% bound. Free fatty acids are noxious, form soaps, dissolve membranes, oxidize becoming rancid, none of which occurs when they are tightly bound to albumin. Retinone, a hormone ..... and testosterone, an anabolic steroid, have undesirable effects on many cells, but can be safely and selectively delivered to their target tissues by having a receptor for the carrier protein - hormone compolex on the cell surfaces in the target tissues, and allowing for its selective release. Not only do such mechanisms protect the rest of the body from these agents, but much smaller amounts of the agent need to be produced and delivered in order to elicit the physiologically desired response. As a broad generality, most of these solutes which bind to plasma proteins are lipid soluble, and could readily permeate cell membranes everywhere to cause damage, so the binding prevents the noxious effects. The binding also raises the amount carried by blood. The total fatty acid concentration in blood is over 100 times the solubility limit in the absence of binding proteins, so the blood's carrying capacity is hugely increased.

From the situations described in the earlier sections of this chapter it is apparent that most processes influencing diffusion do so by retarding molecular mobility, and it is clear that binding

at a diffusion front *always* retards the rate of entry of the solute into the region. How then can binding *facilitate* diffusion? It is not enough just to point out that binding of a solute also provides for its buffering, stabilizing its availability in fluctuating states; that is not diffusional facilitation. But if the concentration of binding sites is so high relative to the free solute concentration, that the diffusional flux of the complexed solute if faster than the diffusional flux of the uncomplexed or free solute, then one has facilitated diffusion. the facilitation is thus in terms of total flux, not in the velocity of the individual molecules.

Consider the general situation for the diffusion of a solute, *S*, with a concentration *s*, in the presence of a solute *B* to which *S* can bind. The concentrations are functions of time and space, so we designate the concentrations of free solute *S* to be $s = s(x, t)$, of uncomplexed solute *B* to be $b = b(x, t)$, and of the complex *SB* to be $sb = sb(x, t)$. The reaction to form *SB* is

$$S + B \underset{k_{-1}}{\overset{k_1}{\rightleftharpoons}} SB ,$$

$$k_b = k_{-1} / k_1 .$$

Returning to the basic one dimensional flux equation, Eq. 5-5, $J_D = - D \, dC/dx$, first consider the analogous steady state situation for fluxes of free and complexed forms of a solute diffusing in parallel. At any particular point in a plane between a planar source and a planar sink, the steady state flux must be the sum of the fluxes of the two species:

$$J_{total} = J_s + J_{sb} = -D_S \cdot \frac{ds}{dx} - D_{SB} \cdot \frac{dsb}{dx} \tag{5-32}$$

In this equations D_{SB} will ordinarily be much smaller than D_S since *B* is a large molecule compared to *S*. The fraction bound is determined by the concentrations and the affinity, in accord with the equilibrium relationship $s \cdot b / sb = k_{-1}/k_1 = k_b$, where the latter is the dissociation constant, Molar. For a high affinity binding k_b is small, so s / sb is small, and the bulk of S is in the bound form. If the gradients of *s* and *sb* are proportional to their concentrations, then the effective diffusion coefficient for the flux of S, D'_S, is the concentration-weighted average for the two diffusing species:

$$D'_S = \frac{s \cdot D_S + sb \cdot D_{SB}}{s + sb} . \tag{5-33}$$

This expression is correct for the diffusion at any point, and can reexpressed in more refined form to relate to particular circumstances of equilibrium binding or for slower rates of reaction of substrate with binding site, or to more explicitly account for the total concentration of binding sites, b_T.

5-6.1. General aspects of diffusion of solute in the presence of binding sites

Having the perspective provided by the steady-state expressions, now consider the transients in order to reconcile the ideas that binding a diffusing solute *always* retards a diffusion front even

though the same binding site may foster facilitated diffusion. The expressions for the one-dimensional diffusion of the three solutes, *S*, *B*, and *SB* are

$$\partial s/\partial t = -k_1 \cdot s \cdot b + k_{-1} sb - G(s) \cdot s + D_S \, \partial^2 s/\partial x^2 , \tag{5-34}$$

$$\partial sb/\partial t = k_1 \cdot s \cdot b - k_{-1} \cdot sb + D_{SB} \, \partial^2 sb/\partial x^2 , \tag{5-35}$$

$$\partial B/\partial t = -k_1 \cdot s \cdot b + k_{-1} \cdot sb + D_B \, \partial^2 b/\partial x^2 , \tag{5-36}$$

where $G(s) \cdot s$ is a generic term for concentration-dependent consumption of *S*, but in the cases which follow we assume $G(s) = 0$. In these general equations D_{SB} may differ from D_B; but often where *B* is a large molecule compared to *S*, $D_{SB} = D_B$. The equations can then be simplified if at each point in space:

$$b(x, t) + sb(x, t) = b_T(x, t), \tag{5-37}$$

where b_T is the total concentration of *B* and *SB*. In the case where $D_{SB} = D_B$ then b_T is constant.

5-6.2. Diffusion in the presence of immobile binding sites ($D_B = D_{SB} = 0$)

Situation 1. Transients in solute concentrations *s*.

Only *S* diffuses, but the binding of *S* by *B* retards the flux of *S*. We assume that *S* is not consumed [$G(s) = 0$]. We make the additional assumption that the total binding site concentration b_T is uniform in space. The local concentrations of *S* and *SB* are changing only through the diffusional flux of *S,* as is seen by summing Eq. 5-34 and Eq. 5-35:

$$\partial s/\partial t + \partial sb/\partial t = D_S \, \partial^2 s/\partial x^2 . \tag{5-38}$$

When the binding rate, k_1, s^{-1} and unbinding rate, k_{-1}, moles $\cdot$ s^{-1}, are both fast relative to the diffusional flux, one can assume instantaneous equilibrium binding:

$$s \cdot b/sb = k_b = k_{-1}/k_1 . \tag{5-39}$$

Following Safford and Bassingthwaighte (1977), using the chain rule to estimate $\partial sb/\partial t$:

$$\frac{\partial sb}{\partial t} = \frac{\partial sb}{\partial s} \cdot \frac{\partial s}{\partial t} = \frac{\partial s}{\partial t} \cdot \frac{k_b \cdot b_T}{(k_b + s)^2} . \tag{5-40}$$

Substituting Eq. 5-40 into Eq. 5-38 gives:

$$\frac{\partial s}{\partial t} = \frac{D_S}{1 + k_b b_T/(k_b + s)^2} \cdot \frac{\partial^2 s}{\partial x^2}, \tag{5-41}$$

which thereby defines the effective diffusion coefficient, D'_S, as a function of b_T, and of the local solute concentration, s:

$$D'_S = \frac{D_S}{1 + (b_T/k_b)/(1 + s/k_b)^2}. \tag{5-42}$$

The D'_S applies at each local point along a diffusion front. As $s \to \infty$, $D'_S/D_S \to 1$. When $s = k_b$, $D'_S/D_S = 4/(4 + b_T/k_b)$. The more fixed binding sites, the slower the diffusion. See Fig. 5-16.

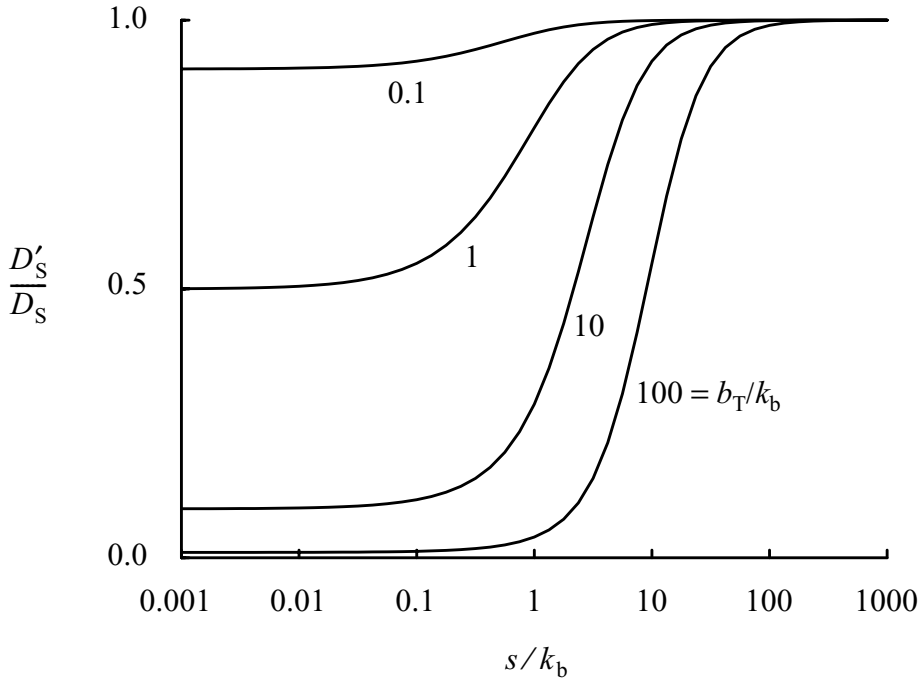

Figure 5-16: Relative effective diffusion coefficient D'_S/D_S versus concentration for S in an invading front when there are *immobile* binding sites B of uniform total concentration b_T (Eq. 5-42). Numbers on curves are values of b_T/k_b. Note that at s/k_b = 1, the values for $D'_S/D_S = 4/(4 + b_T/k_b)$ are 0.9756, 0.8, 0.2857, and 0.0099 for b_T/k_b = 0.1 to 100. Compare these values of D'_S/D_S for native solute entering a field of immobile free binding sites with those for tracer invading a field of pre-equilibrated sites, Fig. 5-19.

Consider the case of an invading front, for example one spreading from a constant source s_o at $x = 0$ when $t = 0$, into a region initially containing no S but containing a uniform concentration of binding sites, b. Then D' is high at $x < 0$, low at $x > 0$ because D'_S/D_S is $\ll 1$ when most S is bound. For a high affinity site (low k_b/b_T), there is a low D'_S ahead of the front, slowing it because of the adsorption of S onto the immobile B. If we call the midpoint of the front the point at which $s = 0.5s_0$, then behind the midpoint D'_S is high. The front is therefore steeper at its mid-level then would be seen with simple diffusion of S in the absence of B.

The steepness of the diffusion front is dependent mainly on the concentration of B in the medium relative to that of S. In Fig. 5-17, left, are shown profiles of $s(x)$ versus x at one time for

three different concentrations b_T/s_0, where s_0 is the concentration at a source of uniform concentration at $x = 0$.

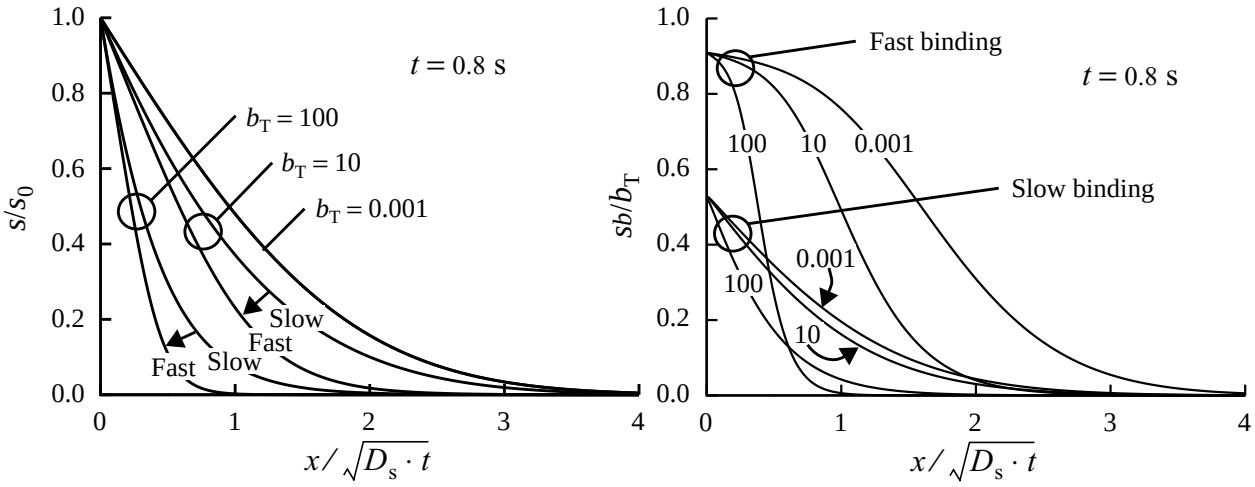

Figure 5-17: Diffusion into a region with immobile binding sites. Concentration profiles for free solute concentration, s, at $t = 0.8$ s after joining a constant source of s with concentration s_0 at concentration $s_0 = 10k_b$ to the left of $x = 0$ at $t = 0$. *Left panel.* The effects of total binding site concentration, b_T, and of the rate of solute binding. Higher concentrations, $b_T = 100$ or 10 mM, retard the diffusion front compared to that with $b_T = 0.001$ mM (the effects of which are indistinguishable from those of $b_T = 0$). Fast binding (with dissociation rate k_{-1} of 1 s^{-1}) retards the front more than does slow binding ($k_{-1} = 0.1$ s^{-1}) because the binding reduces the fraction of s free to diffuse. *Right panel.* The ordinate sb/b_T is the fraction of binding sites occupied. With slow binding ($k_{-1} = 0.1$ s^{-1}) the balance between binding and diffusive movement of solute leaves almost half the sites unoccupied, while with fast binding the fractional site occupancy, sb/b_T, higher. Note that by comparing the profiles in the left and right panels that the profile of sb appears to be ahead of the profile for free unbound s, even though it is only free s that moves. *Parameters for both panels.* $s_0 = 10$ mM, $D_s = 10^{-6}$ cm^2/s, $D_{sb} = 0$, the dissociation constant $k_b = 1$ mM (and $k_b = k_1/k_{-1}$, the off and on rates). All profiles at $t = 0.8$ s.

An invading concentration front is always steepened by binding to an immobile site. Profiles at a succession of times as s diffuses into a stagnant front are shown in Fig. 5-18. The dotted lines show the invasion of s for the same times at a low concentration of b.

Situation 2. Tracer $*s$ in a medium with s and sb constant and uniform.

Both $*s$ and s diffuse, but b and sb do not. For the non-tracer s, $\partial s/\partial t = \partial sb/\partial t = \partial s/\partial x = 0$, but for an added tracer, for example with a step front $-U(x) \cdot s_o$, then $\partial *s/\partial x > 0$. Using the fact that $*sb/*s = sb/s = b/k_b$ for equilibrium binding, and that for the non-tracer $sb/b = b/k_b = b_T/(s + k_b)$, then

$$\frac{\partial^* s}{\partial t} + \frac{\partial^* sb}{\partial t} = D_S \frac{\partial^{2*} s}{\partial x^2}, \tag{5-43}$$

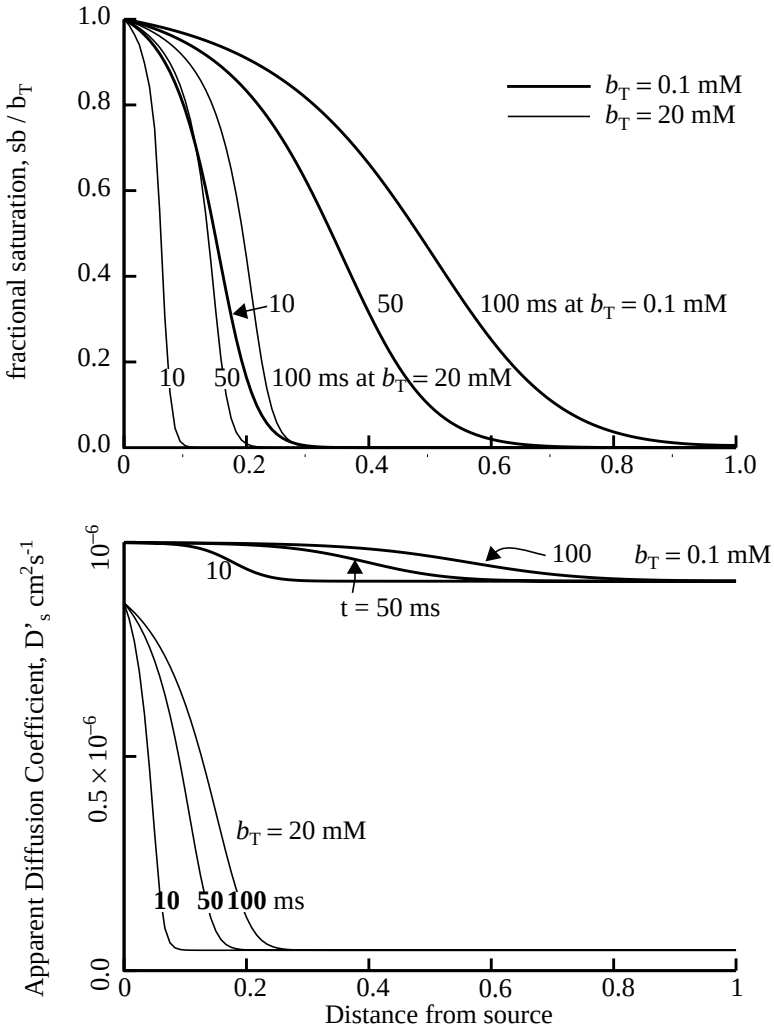

Figure 5-18: Diffusion into a stagnant region containing **immobile** binding sites. Diffusion front positions (*upper*) and apparent diffusion coefficients (*lower*) at three times (10, 50 and 100 ms) after initiating entry of solute *s* into the region. *Parameters:* $s_0 = 10$ mM, $D_s = 10^{-5}$ cm^2/s; $k_b = 1$ mM; $k_{-1} = 1000$ s^{-1} (very fast binding); $b_T = 0.1$ mM, only 0.1 s_0. When b_T is low the effective diffusion coefficient at the advancing front is reduced by less than 10%, whereas with 20 mM b_T the front advances much more slowly with the effective diffusion coefficient reduced to less than 10% of the free solute D_s.

$$\frac{\partial^* s}{\partial t}\left(1 + \frac{b_T}{s + k_b}\right) = D_S \frac{\partial^{2*} s}{\partial x^2} \quad \text{or} \quad \frac{\partial^* s}{\partial t} = \frac{D_s}{(1 + b_T/(s + k_b))} \cdot \frac{\partial^{2*} s}{\partial x^2}, \tag{5-44}$$

which defines

$$D_s'/D_s = \frac{1}{1 + b_T/(s + k_b)} = \frac{s + k_b}{s + k_b + b_T}. \tag{5-45}$$

At very low *s,* at the low-concentration limit as $s \rightarrow 0$, the ratio D_s'/D_s approaches the same limits as given in Eq. 5-42 and Fig. 5-16.

$$D_s'/D_s = \frac{k_b}{k_b + b_T} = \frac{1}{1 + b_T/k_b} . \tag{5-46}$$

The relationships shown in Fig. 5-19 between the effective D_s' for tracer and the concentration of *nontracer s* do not have the same shape as those of Fig. 5-16, being less steep at the inflection points (Fig. 5-19). At $s/k_b = 1$, $D_s'/D_s = 2 / (2 + k_b / b_T)$. At high values of $s \gg k_b$, D_s'/D_s still goes to 1.0.

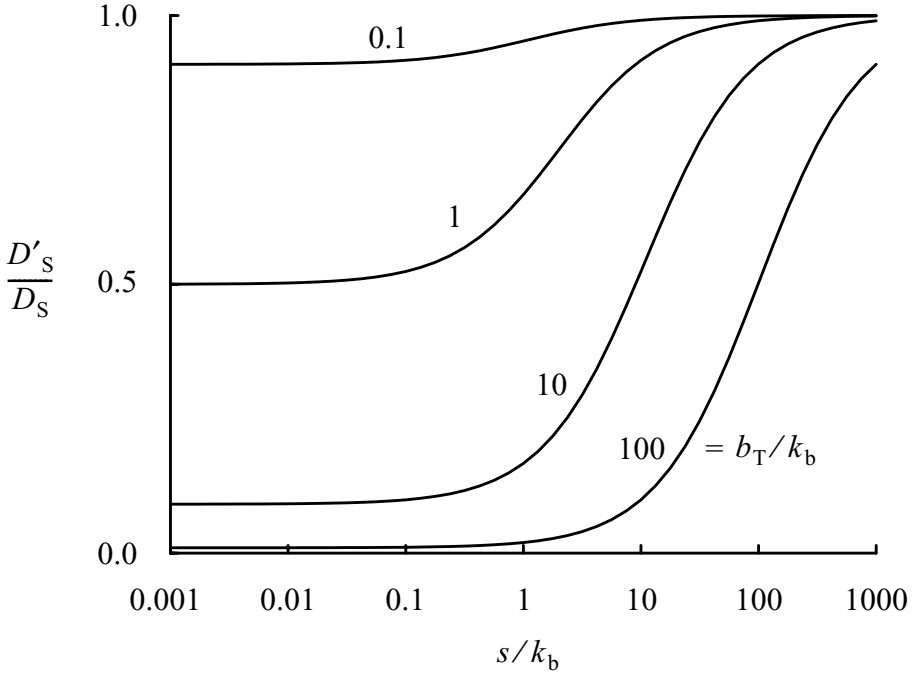

Figure 5-19: Relative effective diffusion coefficient D_s'/D_s for tracer solute *s in a medium with constant equilibrium concentrations of mother solute s and **immobile** binding site b (Eq. 5-45). Note differences from Fig. 5-16. At $s/k_b = 1$, $D_s'/D_s = 2 / (2 + b_T / k_b)$, or 0.952, 0.667, 0.166, 0.0196, all of which are lower than for the invading front of the non-tracer mother solute. These curves are all shifted to the right, higher concentrations, compared to those of Fig. 5-16.

Equation 5-44 and Fig. 5-19 show that D_s'/D_s is dependent only on the concentration of mother solute S and not on the tracer concentration *s. The diffusion front for tracer therefore has a shape defined solely by the random molecular motion of the tracer, so that the fronts are Gaussian, and the effect of the binding sites is to reduce the rate of diffusion, since $D_s'/D_s < 0$.

5-6.3. Diffusion in presence of mobile binding sites (both D_b and D_{sb} finite)

5-6.3.1. Fast binding or equilibrium binding:

Situation 1. **Transients in solute concentrations.** The situation begins with Eqs. 5-34 to5-31. With equilibrium binding, the total flux of s is given by the sum of fluxes of free and bound s:

$$\frac{\partial s}{\partial t} + \frac{\partial sb}{\partial t} = \frac{s}{s + sb} D_s \frac{\partial^2 s}{\partial x^2} + \frac{sb}{s + sb} D_{sb} \frac{\partial^2 sb}{\partial x^2} . \tag{5-47}$$

Given instantaneous equilibration, $k_b = s \cdot b/sb$, and given that $b + sb = b_T$, then this reduces to

$$\frac{\partial s}{\partial t} + \frac{\partial sb}{\partial t} = \frac{s + k_b}{s + k_b + b_T} D_s \frac{\partial^2 s}{\partial x^2} + \frac{b_T}{s + k_b + b_T} D_{sb} \frac{\partial^2 sb}{\partial x^2} . \tag{5-48}$$

The flux by diffusion of $sb + s$ is increased over that by diffusion of the free solute only, since the effective diffusion coefficient is the weighted sum of the two forms in Eq. 5-48.

Situation 2. Tracer transients with s and sb constant. The diffusion of tracer does not affect the free or bound concentrations of solute and therefore, with equilibrium binding, the diffusion coefficient for tracer is the same as that for non-tracer solute (free and bound) at the same location in the solution.

5-6.4. Slow binding kinetics and mobile binding sites

Preceding sections considered the influences of binding on solute diffusion; in case A we saw that immobile binding sites retard solute diffusion, while in case B the mobility of the binding sites could lead to either facilitation or inhibition of diffusion depending on the relative diffusivities, affinities, and concentrations of the solute and binding protein. In both cases we assumed infinitely fast equilibration, that is, equilibrium binding.

When there is slow attachment to the binding site, an invading solute front (a wave of high concentration) advances more quickly than would occur with instantaneous equilibrium binding. For any particular value of the equilibrium dissociation constant, a slow association rate k_1 must be matched by a slow dissociation rate k_{-1} to maintain the same $k_b = k_{-1}/k_1$. Thus, if the off-rate k_{-1} is low, the degree of diffusional facilitation is partially offset by the retardation in release.

In this section we reconsider the factors leading to diffusional facilitation or retardation in the light of slow binding reactions. The relevant partial differential equations are Eqs. 5-34 to 5-37; in this case the solutions are obtained by numerical methods, as described by Barta et al. (2000).

An exemplary situation is the facilitation by albumin of the flux of fatty acid from a constant source across a stagnant layer to a membrane through which the fatty acid permeates and is consumed on the other side. The results portrayed in Fig. 5-20 show diffusional transients in three cases, all leading to the same steady state. In Case 1, left column, the stagnant layer, here given as $L = 50$ μm thick, contains none of the three reacting species, fatty acid, albumin, or the fatty acid-albumin complex, so that all three must diffuse in from the left boundary. In Case 2, all three were in equilibrium in the stagnant layer $0 < x < L$ at $t < 0$, and at $t = 0$ the permeability P of the membrane was switched from zero to its finite value, P_1. In Case 3, albumin, without any fatty

acid, was uniformly distributed throughout the stagnant layer and at $t = 0$ the fatty acid was introduced at the left boundary so that the fatty acid was reacting with the albumin as it diffused.

In all cases, the arrows indicate the sequence of concentration profiles at a succession of times, from 0.1 s to 100 s, by which time a steady state was reached in all cases. The steady states are identical in all columns, though the scales differ from column to column.

Case 1 (Left column): With the region being empty prior to the entry of *S, B*, and *SB* from the source region at $x < 0$, the diffusion and the binding of *S* and *B* and the unbinding of *S* from *B* occur simultaneously. Since *S* has a much higher diffusion coefficient than *B* it invades the empty region more quickly. At $x = L$ the solute *S* permeates the membrane, so that even at 100 seconds the concentration *s* at $x = L$ is lower than at the source at $x = 0$. The diffusion fronts for *B* and *SB* (middle and bottom panels of Fig. 5-20), but their steady-state positions are notably different: the concentration *sb* remains lower at $x = L$ than at $x = 0$, such that $sb(L) / sb(x = 0) = 0.984$, because of the steady loss of *S* across the membrane. The corollary is that the concentration of free binding sites, *b*, must be higher at $x = L$ than at the source, being about 10% higher. The reason that free *B* can be 10% higher while *SB* is only 1.6% lower than at the source is that the K_d is lower than the free ambient concentration of *S,* so most *B* is bound.

Case 2 (Middle column): After pre-equilibration throughout the region, the sudden change in *P* allowing *S* to leave the region through the membrane at $x = L$ diminishes its local concentration to the same steady-state value as in the left column. Likewise the concentration *sb* of the complex diminishes (middle panel), reaching the same steady-state value of $sb / sb_0 = 0.984$. And *b* rises. Note that significant changes occurred within 0.1 s even though the permeability is not very high.

Higher permeabilities drag the concentration *s* down to zero at the membrane if there is no return flux across the membrane.

Case 3 (Right column): Having unfilled binding sites distributed across the region $0 < x < L$ already at $t = 0$ retards the diffusion front for *S* dramatically compared to that in Case 1 with the region empty. At 10 s in Case 3 the profile is not much ahead of that at 0.1 s in Case 1, due simply to the fact that most of the diffusing *S* is captured by binding to *B*. This is seen by the profiles of *sb* being farther to the right of those of free *s* at the same times, since these sites fill before there is much free *S* to diffuse to the right. The concentration of *B* relative to that in equilibration with *S* at the source is initially about 10-fold and then diminishes to the same steady-state values as in the other cases.

To summarize the conditions under which front steepening occurs: (1) $D_s \gg D_{sb}$ so that retardation occurs when *S* is bound, (2) concentrations of $s < k_b$ at the leading part of the advancing front but $s > k_b$ near to the source, and (3) the concentration of binding sites b_T should be of the same order as the concentration *s* so that a substantial fraction of *S* is bound, and (4) the binding/unbinding transformation fluxes should be fast compared to the diffusive fluxes so that the substrate is captured before it goes by.

5-7. Descriptions of biological situations involving these phenomena

5-7.1. Hemoglobin facilition of oxygen transport

The three cases in Fig. 5-20 represent a variety of *in vivo* situations. The third is the commonest: solute enters a region with unfilled binding sites. For example, with sudden oxygenation of RBC previously depleted of oxygen, the diffusion of the first oxygen to enter is retarded by the binding to reduced hemoglobin HHb, forming oxyhemoglobin, $Hb(O_2)_4$,

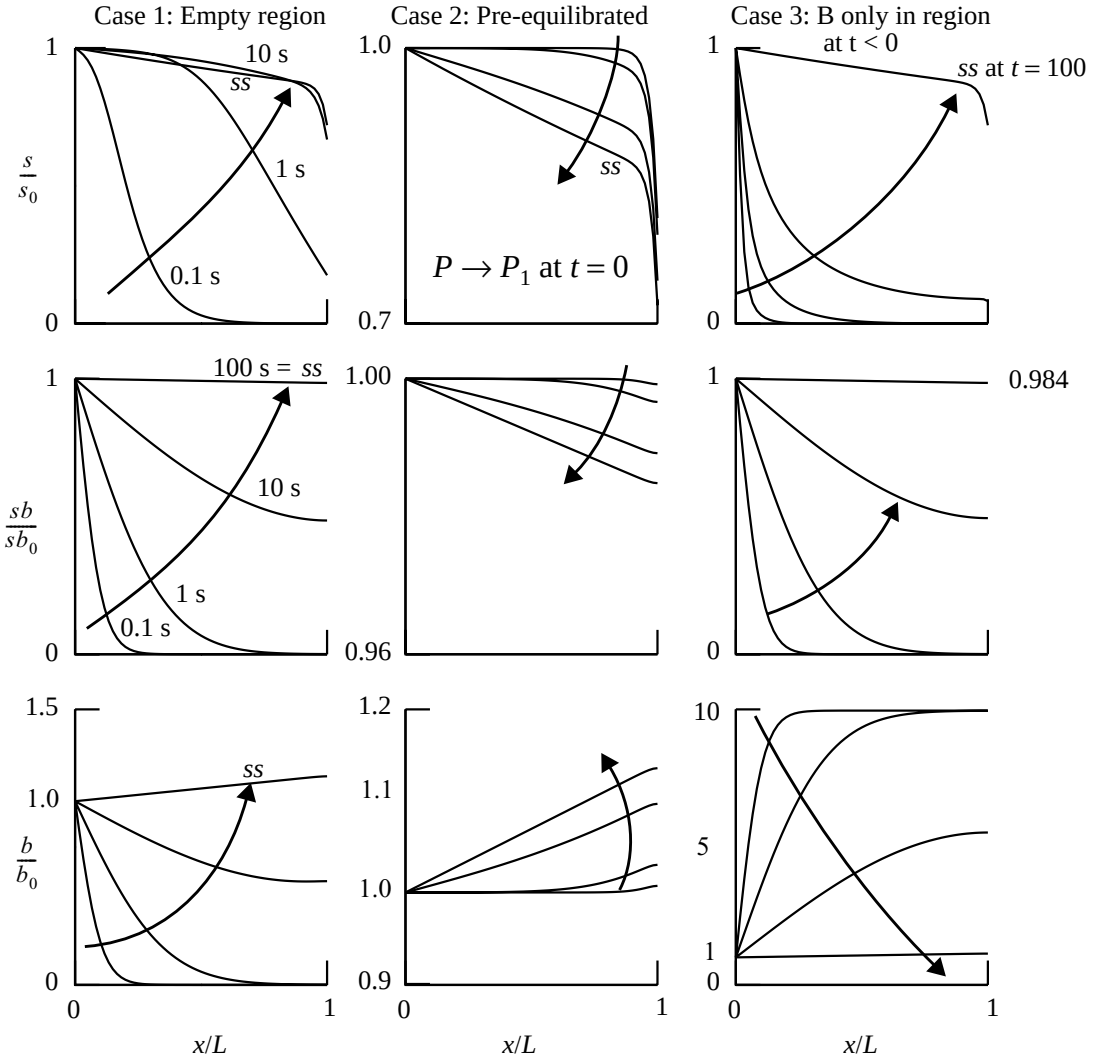

Figure 5-20: Diffusion front formation at successions of times: diffusion of a small solute into or out of a solution with mobile binding sites. Concentrations are plotted versus position, *x/L*, at four times after starting, at $t =$ 0.1, 1.0, 10 and 100 seconds, the succession of times being indicated by the arrows. For all panels $D_s = 5 \times 10^{-6}$ cm^{2}s^{-1}, $D_b = D_{sb} = 9.35^{-8}$ cm^{2}s^{-1}, $k_{on} = 4.73 \times 10^9$ s^{-1}M^{-1}, $k_{off} = 0.142$ s^{-1}, (so that $K_d = 3 \times 10^{-11}$ M) and at the source, $x < 0$, b_T(total) $= 6 \times 10^{-7}$ M, s(total) $= 5.4 \times 10^{-7}$ M. At $x = L$ the membrane permeability, P, was 0.0083 cm s^{-1}. *Left Panel, Case 1*: Solute and binding protein diffuse in together into a solution containing neither at $t = 0$. *Middle panel, Case 2*: A stagnant region contains equilibrated solutes and binding sites at $t = 0$. Membrane permeability was zero at $x = L$ until $t = 0$, then $P \cdot A_m = 1$ ml $\cdot$ s^{-1}, as it was in the other panels. *Right panel, Case 3*: Binding protein B distributed uniformly over $0 < x < L$ at $t < 0$. At $t = 0$, solute S was added at the left boundary. Note the steepness of the profiles in s at early times. In all cases: Steady state was reached by t = 100 s. The concentrations at x/L = 1 were s / s_0 = ??, $sb/sb_0 = 0.984$, and b/b_0 = ??.[Eric, take these from the plot files, the last points for the series at t= 100 sec]

preventing its penetration into the interior of the cell. Oxygen entering later encounters hemoglobin $Hb(O_2)_4$ with filled binding sites just inside the surface layer, and so diffuses quickly as the free O_2, until it encounters HHb with empty binding sites. This causes "front steepening", the creation of a much steeper diffusion front than occurs with simple diffusion into an empty region, as is seen in the right panel of Fig. 5-20. The result is that the front advances almost as a square wave, with the bottom of the front moving at a speed lowered toward that of HHb diffusion, but the top of the front almost catches up to the bottom because in highly saturated $Hb(O_2)_4$, there is much free O_2 whose diffusion is not retarded.

5-7.2. Calcium diffusion and exxcitation-contraction coupling:

Another kinetically relevant diffusional situation is the **entry of calcium into myofilament bundles** after release from the sarcoplasmic reticulum, SR. In muscle fibers the contractile proteins are arrayed in cylindrical bundles a few microns in diameter. These bundles are surrounded by the network of the calcium-storing sarcoplasmic reticulum, SR. With each electrical excitation of the cell, calcium enters the cell at the T-tubular-to-SR junctional region, triggering the ryanodine-sensitive calcium release channels in the SR to open and to flood the neighboring cytoplasm with free calcium, which then diffuses into the myofilament bundles. Within the bundles the Ca^{2+} binds with high affinity to the thin filament protein troponin C, retarding Ca^{2+} diffusion and preventing deeper penetration until the troponin binding sites are filled. Since troponin-Ca^{2+} initiates a sequence of events leading to actin-myosin binding and contraction, the outer filaments of actin and myosin can contract before Ca^{2+} reaches the inner fibers because the Ca^{2+} front is so steep. The result observed by Taylor and Rudel (1970) is that the outer parts of the bundles shorten, reducing sarcomere length by increasing overlap between thick and thin filaments, while the myofilaments in the inner part of the bundle become wavy, compressed as it were, from end to end before undergoing any shortening themselves. Thus the steep radial diffusion front actually resulted in a reduction in efficiency of contraction under the conditions of these particular observations. The authors (Taylor and Rudel, 1970; Costantin and Taylor, 1973) originally attributed the appearance of waviness at short sarcomere lengths to an "inactivation process" occurring selectively in the central part of these large cells of just over 100 μm diameter.

Steep diffusion fronts play a role in many phenomena where there is spread in 2 or 3 dimensions. They exist in oscillating chemical systems such as the Belousov-Zhabitinsky reaction where reactants are removed by chemical reaction, giving sharp concentration profiles. Calcium waves inside cells are closely related. Whether or not signaling cascades, with their high amplification of product formation rates, result in intracellular waves of reactants can only be surmised at this point, but the situation lends itself to steep diffusion fronts whenever there is release of substances which must subsequently be bound or reacted to produce their effect.

5-7.3. Diffusion of calcium through tissues with binding sites :

Use fig from Safford and JB 1977 bioph j #137 fig 1 and fig 7
This is a situation analogous to one with fixed binding sites. Given a Barrer-type experiment, as in Fig. 5-6, instead of examining intratissue concentration profiles one has only the rising time course of concentrations in the unlabeled chamber, $C_R(t)$, for estimating the parameters of the diffusional system. Tissue sheets are usually non-uniform; the equations need therefore account for: heterogeneity of path lengths, diffusion into sequestered regions, volumes or binding affinities

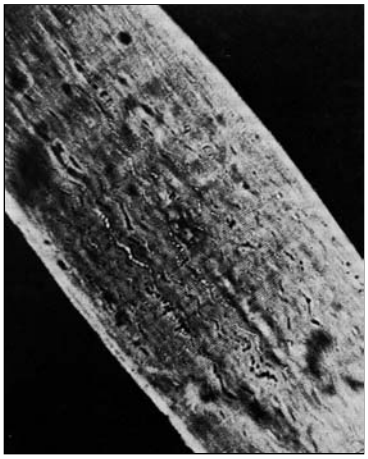

Figure 5-21: Delayed activation of central myofilaments of a myofilament bundle in frog skeletal muscle, *Rana temporaria*, causing waviness of the central fibrils. (From Figure 2 of SR Taylor, 1974, reprinted from J. Physiol. with permission.)

in those regions, and both intracellular and extracellular space. Following the derivation from Goodknight and Fatt (1961 #2251) for oil shales.....??

The key to the experiments and analysis is the simultaaneous use of a set of tracers that give complimentary information: e.g. a neutral solute that undergoes no binding and does not enter cells, e.g. sucrose, a solute that enters the total water space and is not bound, and the solute of interest which is being tested for binding and the affinity of any binding sites.

5-7.4. Transport of organelles along nerve axons by motor proteins plus diffusion:

Motor proteins move large particles, organelles and vesicles, from the body of the neuron toward the end of the nerve up to a meter away, a remarkable process and a long enduring mystery. Now we know that similar events occur in all cells. There is directionality to it; most kinesins move items centrifugally, dynein moves them centripetally. ATP is used to drive the motion, one ATP per step, along a microtubule. A microtubule is a multistrand fibre where each strand is a tubulin polymer; a thirteen strand microtubule is about 25 nm diameter, and the tubulin α/β dimers are 8 nm units. The microtubules are up to 500 μm long, rather stiff, and highly labile, growing and shrinking dynamically with a half life of about 10 minutes. They have direction, the "minus end" being nearer the cell center or neuronal body, the "plus" end going toward the cell membrane or the axonal terminal synapse. The plus end grows at about three times the rate of the minus end.

The general process of translocation along the microtubule is: (1) a kinesin with a special affinity for a particular type of vesicle or organelle binds to it; (2) the kinesin binds to the tubulin, thus linking the cargo to the conveyor belt; hydrolysis of one ATP to ADP moves the kinesin and cargo along by 1 dimer, 8 nm distance; (3) the free particle can diffuse randomly; (4) in cells, unless the microtubules are stabilized by a drug from the Pacific Yew tree, taxol, they disassemble, losing dimers from the ends of the polymers, with an average lifetime of 10 minutes, so that the kinesin and its cargo are turned lose to diffuse again. Friedman and Craciun (2005) define a model for this process in an axon considering 3-dimensional diffusion.

Problem: Write a set of partial differential equations for axonal transport of vesicles of acetylcholine being carried to a synaptic junction at the end of a motor nerve. Given a free diffusion coefficient for vesicles of 0.1 $\mu m^2\ s^{-1}$, a rate of kinesin binding to the vesicle of 2 s^{-1} and

a release rate of 0.5 s^{-1} , a rate of cargo-loaded kinesin binding to the tubulin microfilament of 1 s^{-1} and a release rate of 0.1 s^{-1} , and a forward velocity of 0.5 μm s^{-1} for kinesin along the microtubule: (1) How many ATPs are used per μm? (2) Given a square wave labeling of vesicles from $x = 0$ to $x = 100$ μm at t = 0, what are the concentration profiles for bound and for free vesicles at 1, 10 and 100 seconds? After 10 seconds, what fraction of vesicles are linked to microtubules and what fraction are diffusing, with or without kinesin attached? (4) How much ATP was used by 100 seconds? (5) Given that no taxol was used, what was the average number of microtubules encountered by a vesicle being carried 100 μm?

5-8. Chapter summary

Diffusion is due to random thermal molecular motion. It is enhanced in bulk media by raising temperature and lowering fluid viscosities. Frictional forces retard diffusion; these are larger for larger molecules, in higher viscosity solutions, and in hindering media such as pores or gel matrices.

Transmembrane diffusion of non-electrolytes. To penetrate cell membranes, hydrophilic molecules must be small. In general they don't get across without either facilitating transporters or specialized ion-selective channels. Even for water there is a specialized transmembrane protein facilitating its flux: aquaporin. However, L-glucose (3.6 Å radius) and other inert monosaccharides can slowly enter cells. The cell substrate D-glucose enters much faster, but via a facilitating transporter. Large molecules must be lipid soluble to penetrate. Fastest penetration occurs for molecules which are both small and lipid soluble (CO_2). There is much variation with cell type and species.

Transmembrane diffusion of electrolytes. Electroneutrality must be maintained. A positive ion will not pass through a membrane without a negative ion, unless it exchanges for another positive ion. Membranes are usually charged, and pore edges may repel an ion or accelerate it through the pore. Transmembrane potential differences provide another driving force. See Ch.7.

Diffusion with binding. Diffusion in the presence of binding sites is complicated, depending on the concentrations of sites and on their mobility. With high fractional binding, diffusional facilitation can occur even when the sites are less mobile than the free solute, as with hemoglobin facilitation of oxygen diffusion. Immobile binding sites tend to cause "front steepening" and retardation of solute penetration. The binding sites act as buffers of solute concentration and enlarge the effective volumes of distribution of solute.

5-9. Problems

1. Given the composition of air as 21% O_2 and 79% N, calculate the density of dry air at the freezing point of water and 1 atmospheric pressure (760 mmHg), that is, STPD, standard temperature and pressure, dry. (Hint: Use molecular weights, and the volume of 1 mole of gas at STPD, 22.4 liters.)

2. Using the viscosity of air from a reference source (please provide), estimate a diffusion coefficient for water in air and for methyl salicylate or levomenthone in air.

3. A solute has an apparent permeability of 5 cm/s in the RBC membrane. Estimate the effective diffusion coefficient in the lipid portion of the bilayer, assuming that it is the impeding part of the barrier to exchange. How do you interpret the result?

4. The diffusion coefficient for a solute in a thick membrane in a dialyser system is 0.1×10^{-6} $cm^2 s^{-1}$. Given a membrane thickness of 100 microns and a partition coefficient of 5 for the solute in the membrane compared to the plasma, what is the membrane permeability in cm/s?

5. Diffusion of solute from a source into a medium containing binding sites results in steep diffusion fronts under some circumstances. Define the circumstances. Write equations for the system. Sketch a relationship between steepness of the diffusion front and each of some parameters which govern the steepness.

5-10. Further readings

Classic textbooks are those of Crank (1975), or Carslaw and Jaeger (1959), particularly for heat diffusion, of Jost (1960), and of Bird, Stewart and Lightfoot (1960, 2001). These have no coverage of biology but describe a wide variety of physical situations. The Bird, Stewart and Lightfoot texts are particularly good on deriving the ideas from first principles.Cussler

More biologically oriented are works by Fall et al. (2002) and James D. Murray (1990). Movement in hindered media are discussed by Comper in two volumes (1996a, 1996b). Porous transport, a specific type of hindering, will be covered in Ch. 6. Combined convection and diffusion will be brought up in several later chapters.

5-11. References

Agre P, Preston GM, Smith BL, Jung JS, Raina S, Moon C, Guggino WB, and Nielsen S. Aquaporin CHIP: the archetypal molecular water channel. *Am J Physiol Renal Physiol* 265: F463-F476, 1993.

Barrer RM. A new approach to gas flow in capillary systems. *J Phys Chem* 57: 35-40, 1953.

Barta E, Sideman S, and Bassingthwaighte JB. Facilitated diffusion and membrane permeation of fatty acid in albumin solutions. *Ann Biomed Eng* 28: 331-345, 2000.

Bean CP. The physics of porous membranes: neutral pores. *Membranes: Macroscopic Systems and Models* , edited by Einsenman G. New York: Dekker, 1972, p. 1-54.

Comper WD (Editors). *Extracellular Matrix, Volume 1* Amsterdam: Harwood Academic Publishers, 1996, 476 pp.

Comper WD (Editors). *Extracellular Matrix, Volume 2* Amsterdam: Harwood Academic Publishers, 1996, 386 pp.

Costantin LL and Taylor SR. Graded activation in frog muscle fibers. *J Gen Physiol* 61: 424-443, 1973.

Crank J. *The Mathematics of Diffusion, 2nd edition* Oxford: Clarendon Press, 1975.

Curry FE. Mechanics and thermodynamics of transcapillary exchange.. *Handbook of Physiology, Sec. 2 The Cardiovascular System. Vol. 4, Microcirculation* , edited by Renkin EM and Michel CC. American Physiological Society: Bethesda, Maryland, 1984, p. 309-374.

Cussler, Edward L. *Diffusion. 2nd Edition*.Cambridge University Press. 1997 (not in biblio)

Deen WM. Hindered transport of large molecules in liquid-filled pores. *AIChE J* 33: 1409-1425, 1987.

Cussler, Edward L. *Diffusion. 2nd Edition*.Cambridge University Press. 1997 (not in biblio)

Maxwell, J. C. A treatise on electricity and magnetism. Volume 1 Oxford UK Clarendon Press, 1873

Nugent LJ and Jain RK. Pore and fiber-matrix models for diffusive transport in normal and neoplastic tissues. *Microvasc Res* 28: 270-274, 1984.

Patlak CS and Fenstermacher JD. Measurement of dog blood-brain transfer constants by ventriculocisternal perfusion. *Am J Physiol* 229: 877-884, 1975.
Redwood WR, Rall E, and Perl W. Red cell membrane permeability deduced from bulk diffusion coefficients. *J Gen Physiol* 64: 706-729, 1974.
Safford RE and Bassingthwaighte JB. Calcium diffusion in transient and steady states in muscle. *Biophys J* 20: 113-136, 1977.
Safford RE, Bassingthwaighte EA, and Bassingthwaighte JB. Diffusion of water in cat ventricular myocardium. *J Gen Physiol* 72: 513-538, 1978.
Saxby, 1923?? Need to find this
Schnitzer, J. E. Transport functions of the glycocalyx, specific proteins, and caveolae in endothelium. In Whole Organ Approaches to Cellular Metabolism. Ed. by Bassingthwaighte, Goresky, and Linehan. Springer 1998, pp31-69.
Suenson, M., D.R. Richmond, and J. B. Bassingthwaighte. Diffusion of sucrose, sodium and water in ventricular myocardium. Am.J. Physiol. 227: 1116-1123, 1974
Taylor SR and Rudel R. Striated muscle fibers: inactivation of contraction induced by shortening. *Science* 167: 882-884, 1970.
Taylor SR. Decreased activation in skeletal muscle fibres at short lengths. *The Physiological Basis of Starling's Law of the Heart. Foundation Symposium 24* . Amsterdam: Elsevier, p. 93-116., 1974.
Tong J and Anderson JL. Partitioning and diffusion of proteins and linear polymers in polyacrylamide gels. *Biophys J* 70: 1505-1513, 1996.

5. Diffusion and diffusion coefficients

1. Diffusion of solute and uniform medium containing binding sites
   A. Immobile binding site ($D_B = D_{SB} = 0$).
      Situation E1. Transient for solute *S.*
      Situation E2. Tracer **S* diffusion with *s* and *sb* constant.
   B. Mobile binding site ($D_B = D_{SB} > 0$).
      Situation E1. Transients for *S* with binding site *B* mobile.

Situation E2. Tracer *S transient with s and sb constant.

C. Effect of slow binding kinetics on diffusional facilitation.

2. Path length heterogeneity.
3. Dead-end pores.
4. Parallel paths:

A. Non-interacting paths.

Interexchanging pathways: Cells uniformly dispersed in ISF.

ADD:
diff coeff in water and air and solvent viscosities
boundary layers, as e.g. in BSL p788
Weisiger intrahepatocyte diffusion of FA by flash photobleaching